Investigating Metabolic Regulation of Cancer Stem-Like Cells in the Perivascular Niche

2021 CNF REU Intern: Niaa Jenkins-Johnston

Intern Affiliation: Biomedical Engineering, Cornell University

Abstract:

A population of cancer cells known as cancer stem-like cells, or CSCs, promote mortality in breast cancer by driving metastasis and relapse. These cancer cells interact with the extracellular matrix, other cell types, secreted factors and the perivascular niche, the region directly next to blood vessels. One of the major components of the perivascular niche are the endothelial cells, which secrete factors that regulate stemness properties. The perivascular niche also contains a unique metabolic microenvironment, which affects the metabolic behavior of CSCs. In this study, we created a microfluidic device that features a large central reservoir for collagen, four media reservoirs and two channels for seeding breast cancer and endothelial cells. These microfluidic devices can be used to help better understand the tumor microenvironment and determine how targeting the CSC population could help to prevent or treat late stage breast cancer.

Summary of Research:

Introduction. Metastatic breast cancer presents a significant and unmet clinical need. Breast cancer is the leading type of cancer among women with one in eight women developing breast cancer at some point during their lives [1]. Cancer stem-like cells (CSCs) are known to express specific stem cell markers and demonstrate other properties, such as therapeutic resistance and self-renewal, which allows these cells to evade therapy and repopulate the tumor resulting in relapse [2]. However, the factors that contribute to the emergence of CSCs in tumors are still not well understood.

During metastasis, CSCs move through circulation, spread to distant tissues and interact with the perivascular niche, the region directly next to blood vessels. One of the major components of the perivascular niche are the endothelial cells, which secrete factors that regulate stemness properties such as self-renewal and invasion. The perivascular niche also contains a unique metabolic microenvironment, which affects the metabolic behavior of CSCs. There is currently little research on how endothelial cells together with metabolic diffusion affect the metabolism of tumor cells.

To this end, we plan to use a microfluidic cell culture system (Figure 1). Microfluidics will allow us to precisely control metabolic gradients and spatial organization of cells to uncover how perivascular niche factors affect CSC metabolism and subsequent stemness.
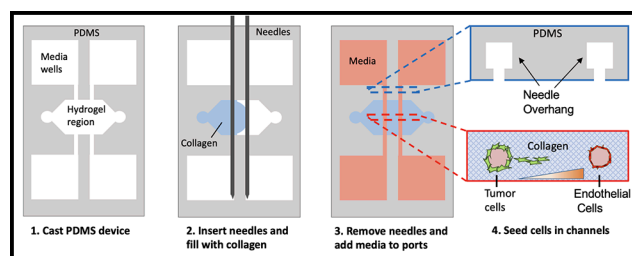

Figure 1: The microfluidic device fabrication process.

Design and Fabrication. The device design consists of three layers: a 100 μm needle buffer layer, a 200 μm needle guide layer, and a 300 μm hydrogel reservoir layer. The needle guide layer helps to keep the needle straight in the channel while the needle buffer layer prevents the needle from touching the bottom of the device. This is essential because cell contact to the plastic or glass device can alter cell behavior.

The microfluidic device mold was fabricated by depositing and exposing three subsequent layers of SU-8 onto a silicon wafer using two fabrication methods: the reverse (Figure 2) and upright (Figure 3) SU-8 processes. Each SU-8 layer of the device design was exposed to UV light using the ABM contact aligner and after all layers were exposed, the wafer was developed.
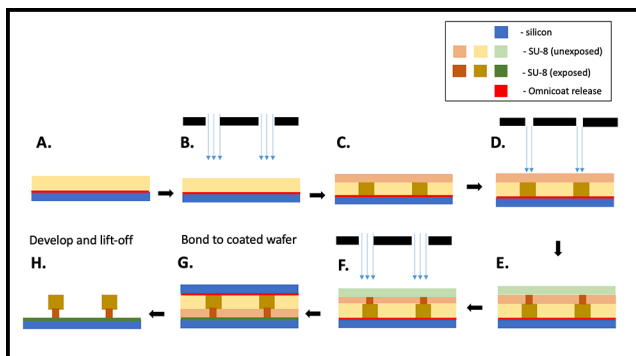
Figure 2: The reverse SU-8 fabrication process steps: a) Coat the wafer with OmniCoat® and SU-8. b) Expose at 350 mj/cm². c) Coat the wafer with a second layer of SU-8. d) Expose devices from 150-600 mj/cm² in 50 mj/cm² increments. e) Coat the wafer with a third layer of SU-8. f) Expose at 450 mj/cm². g) Adhere second wafer to first wafer. h) Develop wafer sandwich and dissolve OmniCoat to remove the first wafer.
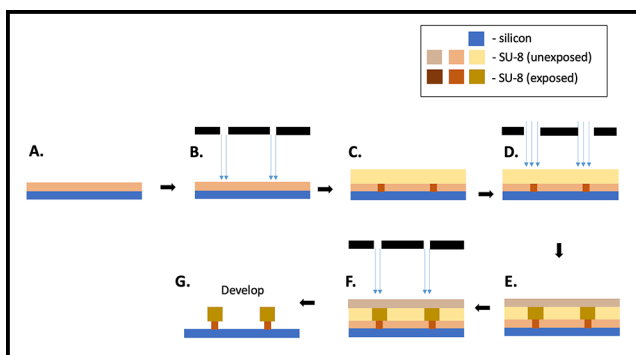

Figure 3: The upright SU-8 fabrication process steps: a) Coat the wafer with SU-8. b) Expose at 300 mj/cm². c) Coat the wafer with another layer of SU-8. d) Expose devices at 150-600 mj/cm² in 50 mj/cm² increments. e) Coat the wafer with a third layer of SU-8. f) Expose at 450 mj/cm². g) Develop wafer.

Device Characterization. The devices were sent to the Biotechnology Resource Center at Cornell University where they were characterized using a CT scanner. The CT scan image shows the devices made from both reverse and upright SU-8 processes. The reverse SU-8 process produced the necessary overhang in the needle guide layer, though slightly elongated, while the upright SU-8 process produced no overhang at all (Figure 4). It was found that the needle buffer and guide had a thickness of about 418 μm, which was close to our estimated 400 μm, while the total thickness of the device is around 745 μm, slightly larger than the 600 μm we had proposed.

Conclusions and Future Steps:

The next phase of this project is to finalize the device fabrication process in order to maximize the effectiveness of the devices. Then, we will cast the PDMS device, insert needles into the channels to fill the collagen reservoir, fill the media reservoirs and lastly seed the channels with tumor and endothelial cells (Figure 1). To increase the strength of the bond between the wafer and substrate, and minimize loss of devices during wafer transfer, we plan to use a substrate bonder. By using metabolic gradient experiments and completing cell culture experiments in our devices, we hope to learn more about the behavior of CSCs and how their properties are affected by the perivascular niche.

References:

[1] SEER Cancer Stat Facts: Female Breast Cancer. National Cancer Institute. Bethesda, MD, https://seer.cxancer.gov/statfacts/html/breast.html.

[2] Yoo, Y. D., Han, D. H., Jang, J. M., Zakrzewska, A., Kim, S.Y., Choi, C.Y., Lee, Y. J., and Kwon, Y. T. (2013). Molecular characteristics of cancer stem-like cells derived from human breast cancer cells. Anticancer research, 33(3),763-777.
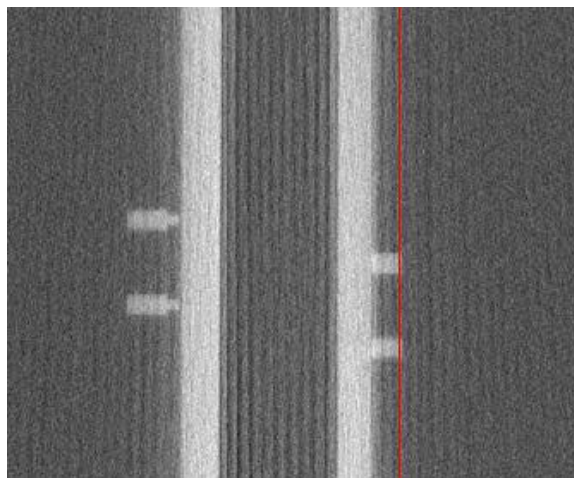
Figure 4: The CT scanner image of the devices from both the reverse (left) and upright (right) SU-8 fabrication methods.

Generating Microfluidic Devices to Study Confined Migration of Cancer Cells

2021 CNF REU Intern: Elisabeth Wang

Intern Affiliation: Biological Sciences and Music, Cornell University

CNF REU Principal Investigator: Jan Lammerding, Meinig School of Biomedical Engineering, Weill Institute for Cell and Molecular Biology, Cornell University

CNF REU Mentor: Richa Agrawal, Biochemistry, Cell and Molecular Biology, Cornell University

Primary Source of Research Funding: 2021 Cornell NanoScale Science & Technology Facility Research Experiences for Undergraduates (CNF REU) Program via National Science Foundation under Grant No. NNCI-2025233

Contact(s): emw239@cornell.edu, jan.lammerding@cornell.edu, ra664@cornell.edu

Primary CNF Tools Used: Heidelberg mask writer - DWL2000, Hamatech-Steag HMP900 mask processor, SÜSS MA6-BA6 contact aligner, Hamatech hot piranha, MVD 100, Anatech plasma asher, Unaxis 770 deep silicon etcher / Oxford Cobra ICP etcher

Abstract:

During metastasis, cancer cells spread from a primary tumor to distal sites. As they travel through interstitial environments, they compress their nucleus to fit through confined areas smaller than themselves. Nuclear deformation can put stress on the cells and have consequences such as nuclear envelope rupture and DNA damage. To study changes induced in cancer cells due to confined migration, polydimethylsiloxane (PDMS) microfluidic devices can simulate the intermittent confinement of an *in vivo* environment. The goal of this research was to create devices which allow for time-lapse imaging and enable collection of cells that had successfully performed confined migration for other characterization. We fabricated devices with constriction areas consisting of a field of heterogeneously spaced pillars by using photolithography techniques to create a wafer with the features for the devices, then creating devices from a PDMS casting of the wafer. We seeded HT1080 fibrosarcoma cells in the devices and allowed them to migrate through the constrictions for up to six days. A study of the cells migrating through the devices over 12 hours showed successful migration. However, over six days, the progress of the cells stalled, possibly due to limited nutrient supply in the confined environment. Overall, the devices successfully model cancer cell migration in a heterogeneous environment, and will be useful for time-lapse microscopy and short-term studies.

Summary of Research:

Cancer cells spread from primary tumors to distal sites during metastasis, which contributes to up to 90% of all cancer-related deaths [1]. As they travel through extracellular matrices, they often must compress their nucleus to fit through tight interstitial spaces [2]. The force required to squeeze through the confined environments can have various consequences for the cells. These effects can include DNA damage from either nuclear deformation that causes increased replication stress [3] or nuclear envelope rupture that allows contents of the cytoplasm and nucleus to mix uncontrollably, leading to greater instability and causing the cancer to advance [4]. However, the full extent that the cells are affected by confined migration is still poorly understood.

To better understand the consequences of confined migration on cancer cells, we designed and fabricated polydimethylsiloxane (PDMS) microfluidic devices with precisely defined confined areas. Previous microfluidic device designs had two main limitations: (1) successive constrictions did not resemble the heterogeneous

confinement of tissues, and (2) the small constriction area limited the number of cells for analysis. Our new device designs included the following improvements: (1) the constriction area consisted of a "heterogeneous field" of pillars with varying spacing, which is more physiological (Figure 1), and (2) the constriction area expanded by
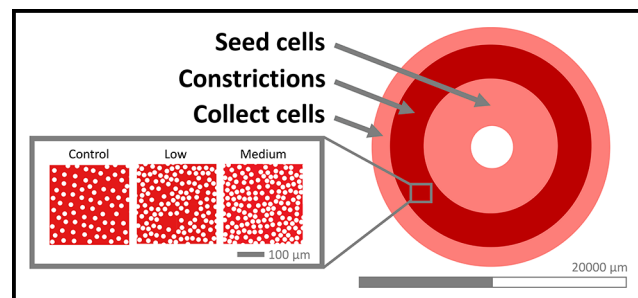

Figure 1: Randomized pillar device design showing the seeding, constriction, and collection areas. Pillars were 5 µm tall and 15 µm in diameter. Modified from Richa Agrawal, submitted to Methods in Molecular Biology.
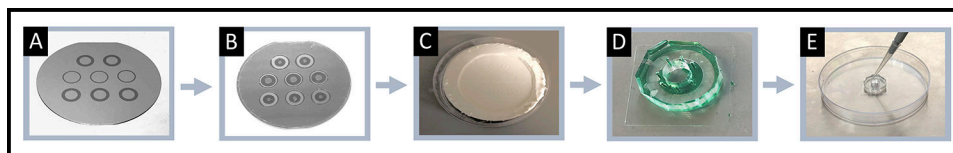
Figure 2: Fabrication workflow for microfluidic devices. (A) First layer of wafer: features for constrictions. (B) Second layer of wafer: features for seeding and collection areas. (C) PDMS casting from plastic mold created from wafer. (D) Devices and seeding ports cut out, then bonded to glass. (E) HT1080 fibrosarcoma cells seeded into device.

100-fold so more cells can be collected after migrating. In addition, the devices have randomized pillars with varying densities, including a relatively "low density" control, to simulate increasing degrees of confinement (Figure 1).

Fabricating microfluidic devices involved making a silicon master mold with two layers. The first layer used reactive ion etching in the Oxford Cobra etcher to create a 5 μm tall constriction area, and the second layer consisted of SU-8 photoresist for 250 μm tall seeding and constriction areas. Microfluidic devices were cut out from a PDMS casting of the wafer and bonded to glass (Figure 2).

Time-lapse imaging of the devices over 12 hours showed that the cells migrate through the constrictions and travel the fastest in the devices with lower pillar densities (Figure 3). Migration was also tracked over several days in another set of devices, and the cells' progress was measured by studying the leading edge of cells. The cells advanced through all of the devices over the first five days, but the average distance from the seeding area decreased on the sixth day, likely due to insufficient nutrient supply that caused some cell death (Figure 4).

However, overall, the devices successfully model migration through a heterogeneous environment and are suitable for time-lapse microscopy and short-term endpoint studies (< four days).

Future Steps:

Decreased migration through the devices after several days most likely indicated insufficient culture media supply or stress from prolonged vertical confinement. Current efforts are focused on creating a version of the devices with a smaller constriction area (< 500 μm) to help with nutrient supply issues, and increased PDMS adhesion area to ensure sufficient bonding to the glass coverslip. We have also created another device with an increased vertical height from 5 μm to 10 μm to eliminate the possibility that cell death was due to prolonged vertical confinement.

Acknowledgements:

References:

[1] Chaffer, C.L., et al. A perspective on cancer cell metastasis. Science (2011).

[2] Keys, J., et al. Assembly and use of a microfluidic device to study cell migration in confined environments. Methods in Molecular Biology (2018).

[3] Shah, P., et al. Nuclear deformation causes DNA damage by increasing replication stress. Current Biology (2021).

[4] Isermann, P., et al. Consequences of a tight squeeze: Nuclear envelope rupture and repair. Nucleus (2017).
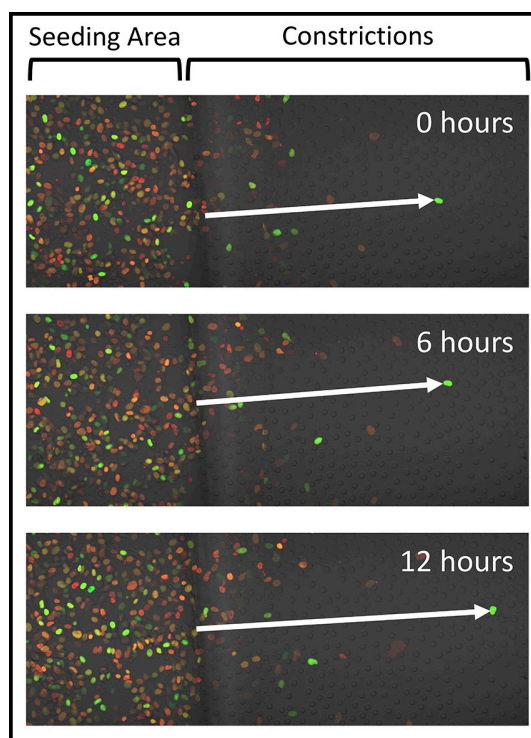
Figure 3: HT1080 fibrosarcoma cells, fluorescently labeled with NLS-GFP (green) and 53BP1-mCherry (red), in a device with a control pillar density region imaged over 12 hours. Migration distance of a single cell inside the constrictions indicated by arrow.
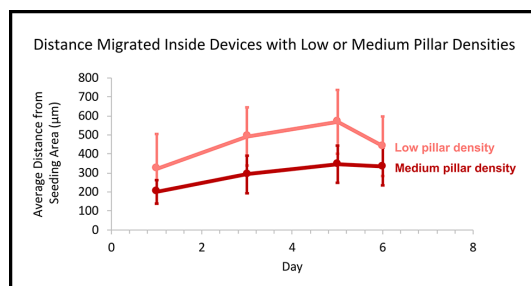

Figure 4: Distance migrated by HT1080 fibrosarcoma cells inside devices with low or medium pillar densities. n=1, 50 cells per timepoint.

Body-on-a-Chip Systems for Drug Development and *in vitro* Interactions

Abstract:

Organ-on-a-chips are microsystems that through tissue-engineering can model human organs, representing both structure and function [1]. Human cell-based multi-organ on-a-chip systems can be used for drug development [2], studying metastasis and chemotherapy. The microscale biomimetics of human organs with organ-organ interactions can be used to model human physiology and disease progression, and thus offer more accurate predictions of human responses to therapeutics and provide mechanistic insights into human diseases. Also, these models can significantly reduce drug development cost and animal usage [3-5]. Currently, we are developing several microfluidic systems, which are fabricated with tools at Cornell NanoScale Facility (CNF) and will be used to study chemotherapeutic toxicity, model cancer cell metastasis, and simulate immune responses.

Summary of Research:

Single-Pass Chip. We have designed and modified a gravity-driven microfluidic model for studying the extravasation of circulating tumor cells (CTC) through endothelium (either primary human liver sinusoidal endothelial cells (LSEC) or human umbilical cord endothelial cells (HUVEC)) into a chamber with HepG2 C3A (liver cells). The frame of this device is made from PMMA layers patterned using a CO_2 laser (VersaLaser VLS3.50), and bonded together using a hot press after a 15 min UV/Ozone (Samco UV& Ozone stripper) exposure at CNF. The propeller stirring lid of the device is fabricated using the Objet30 Pro 3D Printer from the CNF. Clear silicone sheets are also patterned with laser ablation using the VeraLaser CO_2 laser cutter. The stirring is driven by a small stir bar on a magnetic stir plate. This device allows for a continuous operation up to 24 hours while maintaining a constant concentration of CTC and evaluate of the capability of CTC (large and small clusters) from various sources to enter into the liver chamber. [Fig.1]

Unidirectional Chip Devices. We have two unidirectional chip devices (two-chamber and three-chamber chips) for studying the metastasis and drug effects. Chambers are interconnected and perfused with gravity-driven flow at physiological perfusion rates [3-5]. The flow dynamics are characterized computationally and experimentally. Our pumpless gravity-driven flow is created by using a customized programmable rocker where a common media is recirculated between the two reservoirs. Flow rates were measured to be within 15% of the designed values [6,7]. The prototype devices are initially tested for viability where the goal is to maintain a viability greater than 85%.

Two-Chamber Unidirectional Chip. We have developed and modified our original colon-liver two-chamber unidirectional chip system to model CTC liver metastasis. This two organ system interconnects colon and liver
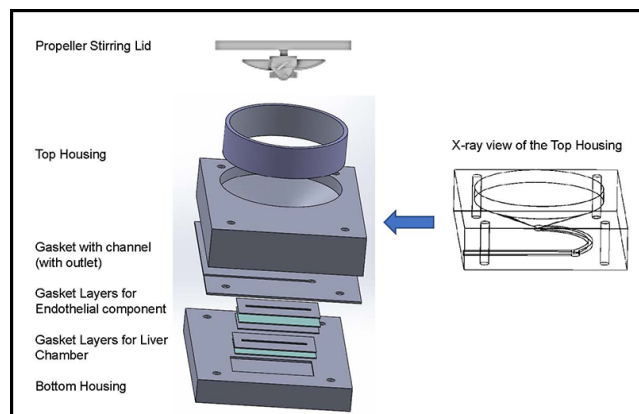

Figure 1: Design of the single pass colorectal/liver metastatic device. Schematic of the single pass device.
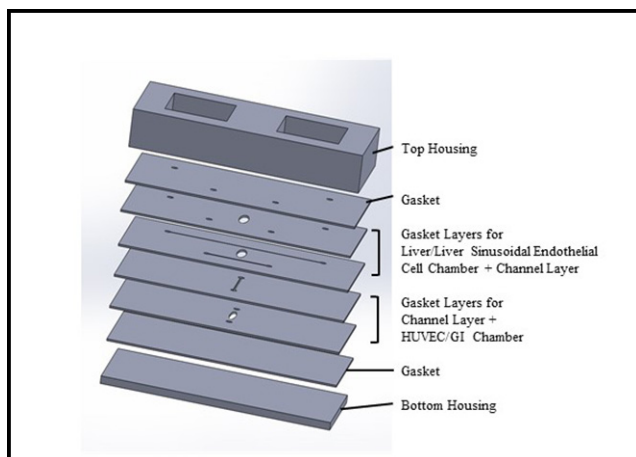
Figure 2: Design of the two-chamber unidirectional chip device. Schematic of the two-chamber unidirectional chip.

Figure 3: Design of the three-chamber unidirectional chip device. Schematic of the three-chamber unidirectional chip.

chambers. The frame of the modified device is milled out of a polycarbonate (PC) sheet at the Cornell University Olin Hall Machine Shop. Clear silicone sheets are patterned with laser ablation using the VersaLaser CO_2 laser cutter to create the chambers, channels and used for sealing the device. For this device, microfluidic channels were etched into silicone gaskets and designed to mimic human blood flow rates [3-5]. Using this colon-liver platform, we are able to incorporate organotypic CTC model into the colon chamber and create a 3D liver construct by incorporating liver cells in a hydrogel into the liver chamber. Here, we are investigating the ability of CTC from various sources to metastasize to the liver chamber. We will investigate the cellular interaction, differentiation, migration and invasion of primary tumors to evaluate contributing factors in CTC metastasis. [Figure 2]

Three-Chamber Unidirectional Chip. A three-organ microphysiological system (tumor-liver-bone marrow chip) [8] that was initially create to study chemotherapeutic toxicity with relevant drug metabolism and hematological side effects is now being used to study metastasis. We modified this device by changing the biological components of the chambers. First, normal colon cells with colon cancer organoids are plated in the colon chamber, HepG2/C3A hepatocytes (in hydrogel) are plated in the liver chamber and then the third chamber (no cells) is used as a control. For this device, microfluidic channels were etched into a layer of poly (methyl methacrylate) (PMMA) and designed to mimic human blood flow rates [3-5]. The silicone cell culture layer and PMMA channel layer were sandwiched between silicone gaskets and outer PMMA housing pieces. All layers were fabricated using the VersaLaser CO_2 laser cutter at CNF. Using this three-chamber platform, we incorporate organotypic CTC model and 3D liver constructs to investigate the metabolic stress due to CRC liver metastasis. We will investigate contributing factors in CTC metastasis by evaluating cellular interaction, differentiation, migration, invasion of primary tumor, metastatic fibroblast tumor microenvironment, and CTC selectivity. [Figure 3]
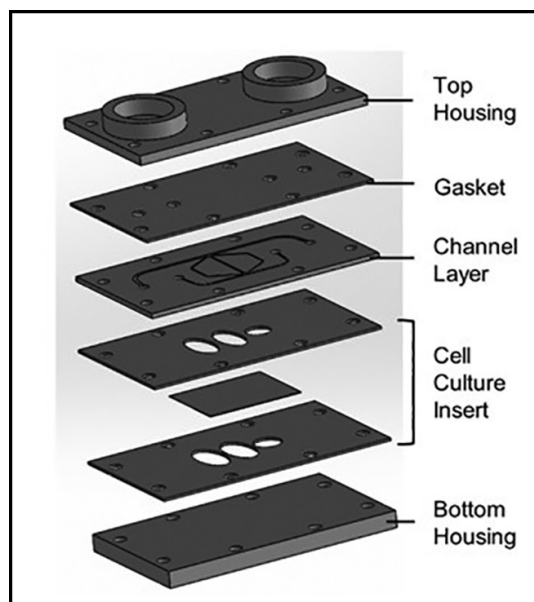
Micromechanical Cantilevers for Cell Motion Transduction. New processes were explored for fabricating silicon micromechanical cantilevers for transduction of cell motion. Process development, including addressing issues of uniformity of devices, continues.

References:

[1] NIH/NCATS. What are tissue chips, and why are they important? https://ncats.nih.gov/tissuechip/about/faq#chips.

[2] Wang YI, Carmona C, Hickman JJ, Shuler ML. Multiorgan Microphysiological Systems for Drug Development: Strategies, Advances, and Challenges. Adv Healthc Mater. 2018;7(2):1701000. doi:10.1002/adhm.201701000.

[3] Price PS, Conolly RB, Chaisson CF, Gross E a, Young JS, Mathis ET, Tedder DR. Modeling interindividual variation in physiological factors used in PBPK models of humans. Crit Rev Toxicol. 2003;33(5):469-503. doi:10.1080/713608360.

[4] Brown RP, Delp MD, Lindstedt SL, Rhomberg LR, Beliles RP. Physiological Parameter Values for Physiologically Based Pharmacokinetic Models. Toxicol Ind Health. 1997;13(4):407-484. doi:10.1177/074823379701300401.

[5] Forrester DW, Spence VA, Walker WF. The measurement of colonic mucosal.submucosal blood flow in man. J Physiol. 1980;299(1):1-11. doi:10.1113/jphysiol.1980.sp013106.

[6] Wang YI, Oleaga C, Long CJ, Esch MB, McAleer CW, Miller PG, Hickman JJ, Shuler ML. Self-contained, low-cost Body-on-a-Chip systems for drug development. Exp Biol Med. 2017; (November); 153537021769410; doi:10.1177/1535370217694101.

[7] Sung JH, Kam C, Shuler ML. A microfluidic device for a pharmacokinetic-pharmacodynamic (PK-PD) model on a chip. Lab on a Chip. 2010;10(4):446. doi:10.1039/b917763a.

[8] LaValley DJ, Miller PG, Shuler ML. Pumpless, unidirectional microphysiological system for testing metabolism-dependent chemotherapeutic toxicity. Biotech Prog. 2021. 37(2). doi: 10.1002/btpr.3105.

Silicon Nitride Cantilevers for Muscle Myofibril Force Measurements

Abstract:

To measure muscle forces in the nano-Newton range, silicon nitride cantilever pairs were manufactured and used. We investigated history-dependent behaviour in cardiac muscle using a single myofibril model. Our experiments demonstrate for the first time that cardiac myofibrils display the same history-dependent properties observed in skeletal muscle, specifically force enhancement following active stretch. The giant molecular spring titin [1] is thought to play a major role in this enhanced force, possibly through interactions of regions of titin with the actin filament. However, titin in cardiac muscle is much smaller than skeletal muscle titin and is missing regions of titin (specifically N2A region) that are suggested to facilitate interactions with actin. We investigated rabbit cardiac myofibrils to see if enhanced force following stretch is present in eight samples. We observed in all tests performed, greater force after stretch compared to force in the isometric condition and at the same sarcomere length. This provides, for the first time, evidence that cardiac muscle displays history-dependent behaviour.

Summary of Research:

The active force produced by skeletal muscle is well described by the Huxley cross-bridge model [2] and the force-length relationship [3] but these well accepted paradigms cannot adequately explain greater force at the identical muscle length when the muscle is lengthened during the contraction (eccentric contraction), compared to a muscle that does not change length (isometric contraction). This history-dependent force has been observed for over 60 years, but no generally accepted mechanism has been put forth to explain it. Recently, titin interaction with other sarcomeric proteins has been proposed as a mechanism and promising work on a mutation mouse model (mdm) has provided evidence that the N2A region of titin is essential for force enhancement [4]. We hypothesize that cardiac muscle will exhibit enhanced force following active stretch because cardiac muscle contains a domain similar to the N2A region (i.e. N2AB) and so cardiac titin will interact with actin, as has been proposed for skeletal muscle.

Myofibrils were harvested from heart ventricle muscle obtained from New Zealand White rabbits and were chemically and mechanically isolated as described in our previous work [5]. Single myofibrils were attached to nanofabricated silicon-nitride cantilevers (stiffness 150 pN/nm) [6] for force measurement at one end of the myofibril (resolution < 0.5 nN), and at the other end, a glass pipette needle attached to a piezo-motor for controlling specimen length (Figure 1).

Forces were divided by the cross-sectional area of the myofibril and reported as stress ($nN/\mu m^2$).
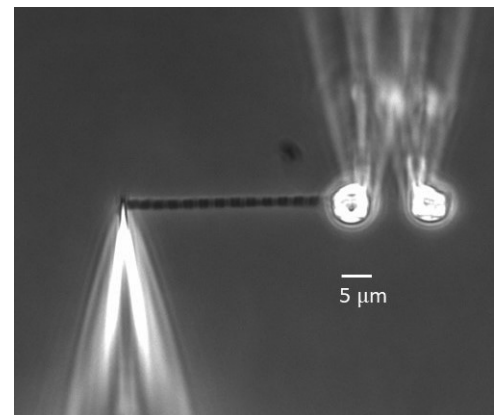

Figure 1: Myofibril attached to a glass needle for stretch-shortening and nano-levers for force measurement. Example of a myofibril with 13 sarcomeres in-series.

Myofibrils (n=8) were stretched passively from an average sarcomere length (SL) of 1.8 μm to 2 μm, held at that length, and then activated by infusing Ca^{+2} and ATP. After 10 seconds, the specimen was shortened to 1.8 μm and held for 20 seconds to allow the force transients to fade and then the specimen was rapidly stretched to 2.0 μm and held. After the stretch force transients faded, the second force measurement was made.

The isometric (SL=2 μm) and eccentric tests (SL=1.8 μm stretched to 2.0 μm) were combined in a single experiment (Figure 2). The force was recorded at two time-points: once at first vertical-red bar (75 seconds) for the isometric condition and then at the steady-state condition following the active stretch (second vertical bar-blue) at 150 seconds into the test. The eccentric stress was normalized to the isometric stress for each test and the residual force enhancement as a percentage increase (RFE) reported (Figure 3).

In all eight experiments, residual force enhancement following stretch was observed, (average increase 20%).

We show here for the first time, force-enhancement in cardiac myofibrils and this work provides insight into the possible titin-actin interaction in the eccentric condition as the mechanism underlying this phenomenon.

References:

[1] Granzier and Labeit. Muscle Nerve. 36:740-755, 2007.

[2] A.F. Huxley, Prog Biophys Biophys Chem.7:255-318, 1957.

[3] Gordon, et al., J Physiol. 184(1):170-92, 1966.

[4] K. Powers, et al. JEB. 219:1311-1316, 2016.

[5] Joumaa, et al. Eur J Physiol. 455:367-371, 2007.

[6] M. E. Fauver, et al. IEEE Trans Biomed Eng 45(7):891-898, 1998.

Figure 2: Isometric and steady-state isometric stress following stretch, for a single myofibril test. The residual force enhancement is formalized to the initial isometric stress.

Figure 3: Residual force enhancement values for each of eight myofibrils tested. The increased stress observed following stretch compared to the isometric stress ranged from 11% to 42%, with a mean value of 20%. RFE is statistically greater than the isometric value, Wilcoxon test, $a=0.05$.

Nanophotonic Standing-Wave Array Trap for Single-Molecule Applications

CNF Project Number: 1738-08

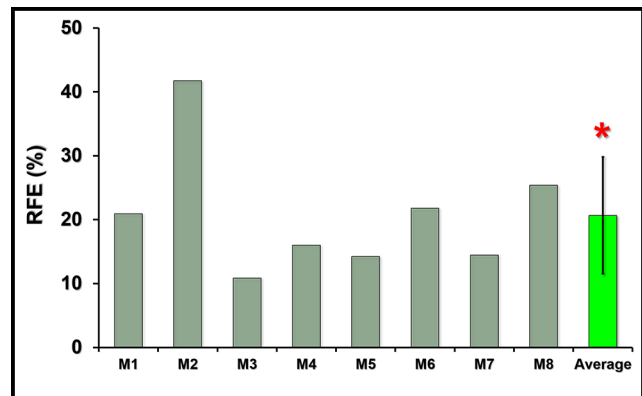**Principal Investigator(s): Michelle D. Wang**

User(s): Yifeng Hong

Affiliation(s): a) Department of Electrical and Computer Engineering, Cornell University; b) Department of Physics, Cornell University; c) Howard Hughes Medical Institute, Chevy Chase, Maryland
Primary Source(s) of Research Funding: Howard Hughes Medical Institute
Contact(s): mdw17@cornell.edu, yh874@cornell.edu
Website: http://wanglab.lassp.cornell.edu/
Primary CNF Tools Used: ASML DUV stepper, Oxford 100 plasma etcher, Oxford 81 etcher, Oxford 82 etcher, Unaxis 770 deep Si etcher, Heidelberg mask writer - DWL2000, SÜSS MA6-BA6 contact aligner, Gamma automatic coat-develop tool, LPCVD nitride - B4 furnace, wet/dry oxide - B2 furnace, AJA sputter deposition, Oxford PECVD, CVC SC4500 odd--even hour evaporator, Zeiss Supra SEM, Zeiss Ultra SEM

Abstract:

As a fundamental tool in single-molecule science, optical tweezers have been used broadly for decades. The Wang Lab has developed a nanophotonic standing-wave array trap (nSWAT) device, which integrates the functions of a conventional microscope-based optical tweezer into a centimeter-scaled chip. Here, we present our latest progress on nSWAT applications, focusing on high enough force generation. This increased force enables us to unzip an array of DNA molecules along the waveguide, thus providing a platform for parallel single-molecule measurements.

Summary of Research:

In the past few years, the Wang Lab has been working on developing the nanophotonic standing-wave array trap (nSWAT) device, aiming for high-throughput single-molecule manipulations and measurements [1-6]. In principle, the nSWAT is generated by the interference of two counter-propagating waves along a single-mode waveguide. Polystyrene beads attached to biomolecules like DNA can be trapped within the antinodes of the near-field evanescent waves at the waveguide surface (Figure 1). As a result, those biomolecules can be manipulated in parallel by modulation of the trapping array. For instance, a simple application of parallel DNA molecule sorting has been demonstrated [2].

To further make use of the nSWAT platform for fundamental single-molecule studies, such as an unzipping assay for protein-DNA interaction, we have to overcome the force limitation of the existing nSWAT. Recently, a more advanced version of the Si_3N_4 nSWAT (operated at 1064 nm laser) [3] has been developed to enhance the maximum trapping force applied to the biomolecules, and includes features such as minimized absorption and bending loss as well as a fastest heater reset time. Increased trapping force enables us to unzip DNA molecules, and expands opportunities to study protein-DNA interaction in a high-throughput manner.
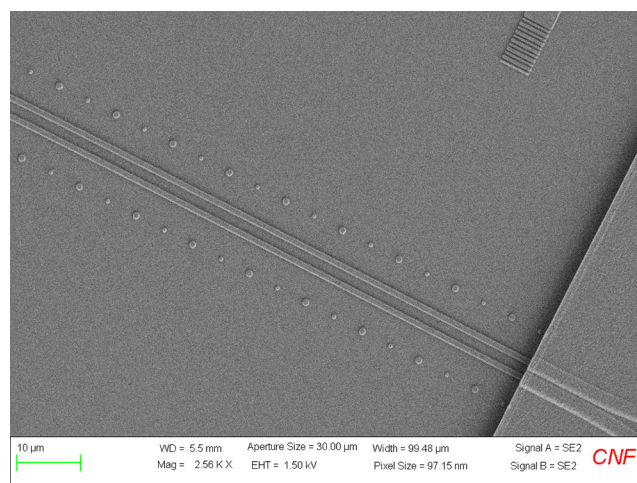

Figure 1: An SEM image of the waveguides at the trapping region (fluid pool). A standing wave is generated along each waveguide, forming a trapping array for 380 nm polystyrene beads. The dot arrays near the waveguides are fiducial marks for monitoring the global drifting during operation. (See cover for more detail.)

So far, this technique has been applied to locate a bound protein with nearly nm spatial resolution, which serves as a benchmark of on-chip optical trapping techniques. We hope this high-throughput technique can become a fundamental tool in other aspects of biological studies.

The achievements based on the nSWAT have led to six publications [1-6]. The latest demonstration of unzipping DNA to map a bound protein has been submitted for publication this year.

References:

[1] J. E. Baker, R. P. Badman, and M. D. Wang, "Nanophotonic trapping: precise manipulation and measurement of biomolecular arrays" WIREs Nanomed Nanobiotechnol. e1477 (2017).

[2] M. Soltani, J. Lin, R. A. Forties, J. T. Inman, S. N. Saraf, R. M. Fulbright, M. Lipson, and M. D. Wang, "Nanophotonic trapping for precise manipulation of biomolecular arrays" Nature Nanotechnology 9(6), 448-452 (2014).

[3] F. Ye, R. P. Badman, J. T. Inman, M. Soltani, J. L. Killian, and M. D. Wang, "Biocompatible and high stiffness nanophotonic trap array for precise and versatile manipulation" Nano Letters 16(10), 6661-6667 (2016).

[4] F. Ye, M. Soltani, J. T. Inman, and M. D. Wang, "Tunable nanophotonic array traps with enhanced force and stability" Optics Express 25 (7) 7907-7918 (2017).

[5] R. Badman, F. Ye, W. Caravan, and M. D. Wang, "High Trap Stiffness Microcylinders for Nanophotonic Trapping" ACS Appl. Mater. Interfaces 11(28), 25074-25080 (2019).

[6] R. Badman, F. Ye, and M. D. Wang, "Towards biological applications of nanophotonic tweezers", Current Opinion in Chemical Biology, 53, 158-166 (2019).

Microfluidics Channels for Zinc Metal Homeostasis

Abstract:

We constructed a custom-made microfluidic device for the control growth of *Escherichia coli* (*E. coli*) colonies in microchambers. The confinement of the cells is achieved by matching the height of the microchambers with the diameter of the *E. coli* cells. The objective of our study is to image *E. coli* strain with fluorescent protein reporters to elucidate the role individual cells play in colonies achieving metal homeostasis.

Summary of Research:

Biological processes in the gut microbiome heavily depend on the harmonious balance between microbial communities and a host. This balance is maintained by chemical and biophysical cues that are exchanged between organisms to coordinate behavior. Zinc is an essential micronutrient for all living organisms [1]. It plays a vital role in protein folding, catalysis, and gene regulation [2]. To regulate the uptake/efflux of metal ions, bacterial cells control the transcription of the protein pumps with metal-responsive transcription regulators that sense the cellular concentration of metal ions.

The purpose of this project is to quantify the management of Zn^{2+} in a microbiome and determine the role the individual cells have in the colony achieving metal homeostasis. As a model system, *Escherichia coli* (*E. coli*) will be used to study community-derived zinc metal regulation. *E. coli* cell's motility and poor adherence to a substrate make it difficult to conduct imaging studies with long time scales. Microfluidics technology is a widely accepted method to study bacterial communities in a controlled environment [3]. A microfluidic platform permits tight control of the nutrients influx and has been successfully used for long-timescale imaging studies [4].

The design of the microfluidic device is shown in Figure 1. This study focuses on community behavior; thus, we chose the width and length of the chamber to be about ~ 200 μm. The depth of the microchamber has been chosen to match the diameter of an *E. coli* cell (~ 1 μm) [5]. The high aspect ratio (200:1) is problematic due to the possibility of ceiling collapse [6] caused by the attractive forces between PDMS and the glass coverslip. Therefore, the roof is supported by regularly spaced pillars. The regularly spaced pillars were designed to have the shape of circles or squares with a diameter or length of 4 or 8 μm.
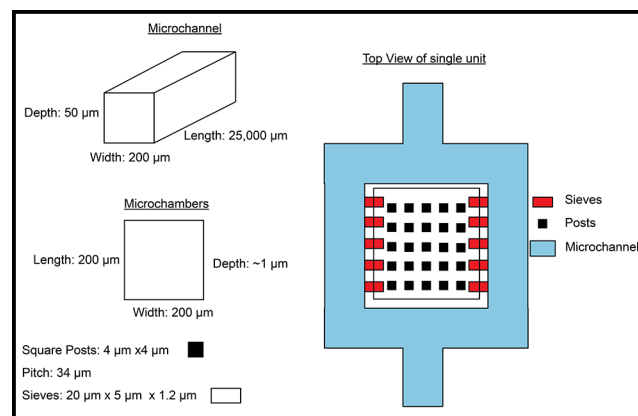

Figure 1: Schematic of the microfluidic device design of the microchannel and microchambers with the desired dimensions.
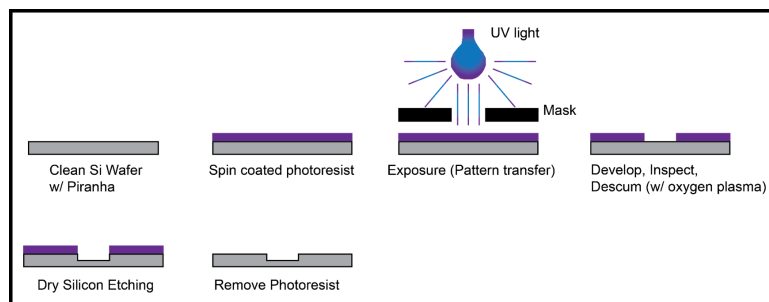

Figure 2: Fabrication scheme of the silicon mold for the microfluidic device.
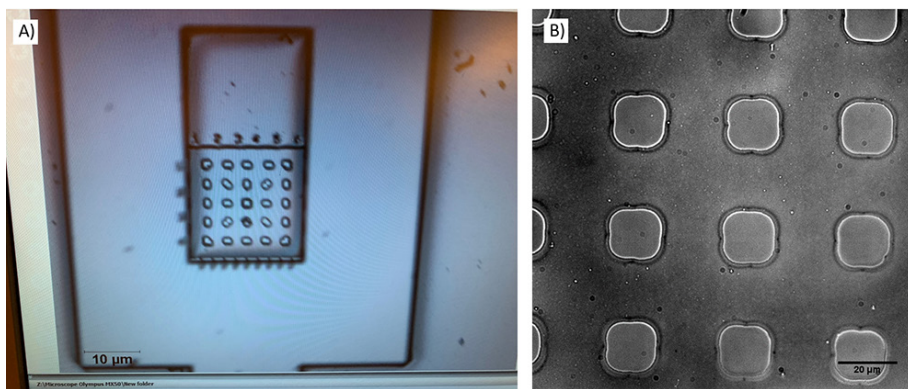
Figure 3: A) A photographed image of a prototype of the microfluidic device. B) Bright-field image of the PDMS posts used to prevent ceiling collapse.
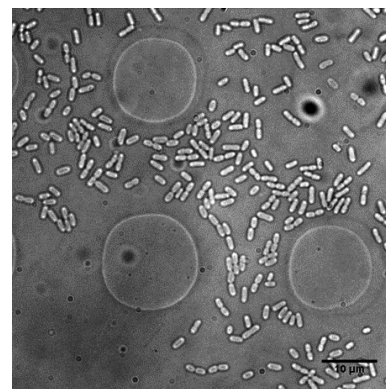

Figure 4: A bright-field image of one growth chamber filled with E. coli *cells*.

The microfluidics devices are constructed using well-established silicon nanofabrication technology. The fabrication scheme is summarized in Figure 2. Briefly, silicon wafers were cleaned with piranha solution from the Hamatech wafer processor. Afterwards, they were spin coated with photoresists. Photoresist was removed 2 mm from the edge of the wafer using the edge bead removal system. The substrate was patterned using a pre-patterned photomask made using the Heidelberg mask writer - DWL2000. The SÜSS MA6-BA6 contact aligner was used for the UV light exposure of the wafer. After developing the wafer and cleaning it with a brief oxygen plasma. The chamber was created by etching about ~ 1 μm of silicon using the Oxford Cobra ICP etcher. The photoresist was removed using the photoresist stripper bath. The height of the chamber was measured using a profilometer. The same process was repeated to create the flow channels; however, the Plasma-Therm deep silicon etcher was used for the etching step to create channels with depths of about 50 μm.

The final step is coating the silicon mold with a hydrophobic molecular monolayer such as tridecafluoro-1,1,2,2-tetrahydrooctyl trichlorosilane (FOTS). An image of the prototype of the microfluidic device is shown in Figure 3A. After casting PDMS on the silicon mold, the microfluidic devices were bonded to coverslips and inspected using a microscope. The brightfield image of the chamber shows a regularly spaced PDMS post preventing the collapse of the ceiling (Figure 3B).

The loading of the cells into the chambers is a challenge. One approach is to increase the gauge pressure inside the devices to inflate the microchannels, and cause the ceiling to bulge up, increasing the height of the channels and allowing the passage of the cells. Reducing the pressure causes the channels to deflate, and the ceilings return to their original height. The brightfield image shown in Figure 4 shows an example of a chamber loaded with *E. coli* using the procedure described previously. The future step is to test this prototype and optimize the conditions for the successful completion of the project.

References:

[1] R. R. Robert B. Saper, Zinc: An Essential Micronutrient. Am. Fam. Physician. 79, 768 (2009).

[2] A. R. Blanden, X. Yu, A. J. Blayney, C. Demas, J.-H. Ha, Y. Liu, T. Withers, D. R. Carpizo, S. N. Loh, Zinc shapes the folding landscape of p53 and establishes a pathway for reactivating structurally diverse cancer mutants. Elife. 9 (2020), oi:10.7554/eLife.61487.

[3] F. Wu, C. Dekker, Nanofabricated structures and microfluidic devices for bacteria: from techniques to biology. Chem. Soc. Rev. 45, 268-280 (2016).

[4] D. Binder, C. Probst, A. Grünberger, F. Hilgers, A. Loeschcke, K.-E. Jaeger, D. Kohlheyer, T. Drepper, Comparative Single-Cell Analysis of Different E. coli Expression Systems during Microfluidic Cultivation. PLoS One. 11, e0160711 (2016).

[5] A. Groisman, C. Lobo, H. Cho, J. K. Campbell, Y. S. Dufour, A. M. Stevens, A. Levchenko, A microfluidic chemostat for experiments with bacterial and yeast cells. Nat. Methods. 2, 685-689 (2005).

[6] Y. Y. Huang, W. Zhou, K. J. Hsia, E. Menard, J.-U. Park, J. A. Rogers, A. G. Alleyne, Stamp collapse in soft lithography. Langmuir. 21, 8058-8068 (2005).

Sample Cells for High Pressure Biological X-Ray Solution Scattering

CNF Project Number: 1940-10

Principal Investigator & User: Richard E. Gillilan

Affiliation(s): Macromolecular Diffraction Facility of the Cornell High Energy Synchrotron Source (MacCHESS), Cornell High Energy Synchrotron Source; Cornell University
Primary Source(s) of Research Funding: National Science Foundation DMR-1829070, National Institutes of Health 1-P30-GM124166-01A1 and NYSTAR
Contact(s): reg8@cornell.edu
Website: https://www.chess.cornell.edu/macchess/hp_more
Primary CNF Tools Used: VersaLaser VLS3.50 engraver/cutter tool

Abstract:

Over 80% of the biomass of Earth consists of organisms living under extreme conditions of temperature, pressure, and chemical environment. As a potentially rich source of new tools and deeper understanding of the history and limits of life, there is much renewed interest in conducting biophysical and structural biological measurements under these types of conditions. We have developed an X-ray transparent, biologically compatible sample environment for conducting small angle X-ray solution scattering at hydrostatic pressures of up to 400 MPa (58,000 psi). The disposable, low-volume cells are designed to allow pressure equalization between the sample and pressurizing medium without excessive flexing of the thin X-ray transparent windows. The current design has been routinely and successfully used at the Cornell High Energy Synchrotron's High Pressure Biology facility (HP-Bio) since late 2019, including a remote "hands-on" training course in April 2021.

Summary of Research:

Though we surface dwellers are rarely aware of it, high hydrostatic pressure is the norm for most of the biomass on Earth. Organisms living in the deep ocean and subsurface experience pressures that can reach beyond 100 MPa (14500 psi). Biomolecules do not merely compress in response to external pressure; they rearrange their structure in informative ways to minimize total volume, including that of the surrounding water [1]. X-ray solution scattering (SAXS) is well-suited to study such changes, but special design considerations are necessary to handle the high pressure.

We recently introduced an easy-to-use SAXS system capable of maintaining up to 400 MPa of hydrostatic pressure on biological samples [2]. The system uses X-ray transparent single crystal diamond windows combined with a quick sample change mechanism (Figure 1A,B). To prevent the pressurizing medium (water) from mixing with the biological samples, we designed disposable laser cut PMMA cells with thin, X-ray transparent 7 μm polyimide film windows. At 400 MPa, the specific volume of water has declined by a significant amount, 11.6%. The chemically inert silicone grease used to seal the cells can flow, allowing pressure between the sample and external pressurizing water to equalize. The cells have also been adapted successfully to hold standard 1.5 mm glass sample capillaries for use in studying phase changes in deep sea lipid samples (Winnikoff and Budin, personal communication, 2021).
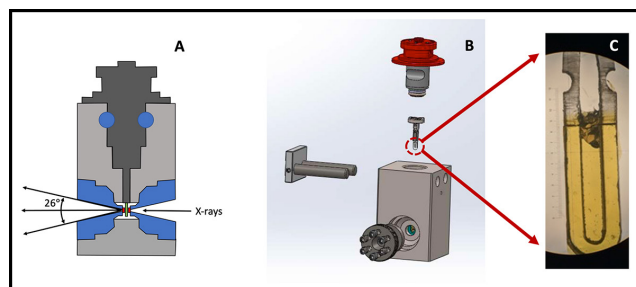

Figure 1: High pressure small-angle solution scattering system. X-rays enter the cell from the right (A) traveling through a single-crystal diamond window, passing through a sealed plastic sample cell at center and emerging from the second diamond window scattered at angles up to 26°. Water is used as a pressure medium. A locking pin and piston-style o-ring system allows easy access to the disposable inner PMMA cell (B), which has 7 μm polyimide windows to minimize X-ray scatter and a grease seal to allow for pressure equalization.

References:

[1] Ando N, Barquera B, Bartlett DH, Boyd E, Burnim AA, et al. 2021. The Molecular Basis for Life in Extreme Environments. Annu. Rev. Biophys.

[2] Rai DK, Gillilan RE, Huang Q, Miller R, Ting E, et al. 2021. High-pressure small-angle X-ray scattering cell for biological solutions and soft materials. Journal of Applied Crystallography. 54(1): 111-22.

Bacterial Mechanics and Mechanobiology

Abstract:

Bacteria naturally experience mechanical forces in the environment. Bacteria experience mechanical forces as they grow and divide, swim in fluids, attach to surfaces, and grow in biofilms. Although it has been well established that mechanical forces are key signals for eukaryotic cell development and physiology, much less is known about the importance of mechanical forces for bacterial cells. This is in part because applying controlled mechanical stimuli to bacterial cells is technically challenging due to the small scale of bacteria (~ 1 μm wide). We developed a microfluidic platform to apply mechanical stimuli to individual, live bacteria cells. We use this microfluidic platform to apply mechanical loads to *E. coli* and *V. cholerae* cells in order to understand how mechanisms of antibiotic resistance respond to mechanical stimuli. Additionally, we use this microfluidic platform in conjunction with finite element modelling to quantify the mechanical properties of the bacterial cell envelope.
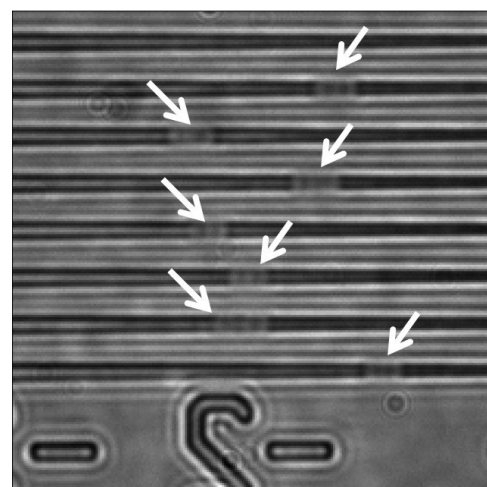
Figure 1: E. coli *cells trapped within the tapered channels of the microfluidic device. Fluid pressure is used to flow the bacteria into the tapered channels.*

Summary of Research:

Our work involves the use of microfluidic devices to apply a mechanical stimuli to individual bacteria. Within our devices, fluid pressure pushes individual bacteria into narrow tapered channels (Figure 1). The bacteria experience mechanical loading from the hydrostatic fluid pressure as well as contact with the tapered channels walls (Figure 2). The amount of mechanical loading a cell experiences depends on the fluid pressure, which is varied strategically within the device. During a single experiment, different cells experiencing different magnitudes of mechanical loading can be observed simultaneously. The bacteria remain alive while trapped in the tapered channels and continue to elongate and divide. Cells remain viable for up to 12 hours in the devices.

Key advantages of this microfluidic platform include minimal sample preparation, no chemical immobilization or labeling, and the ability to analyze hundreds of cells at once [1].
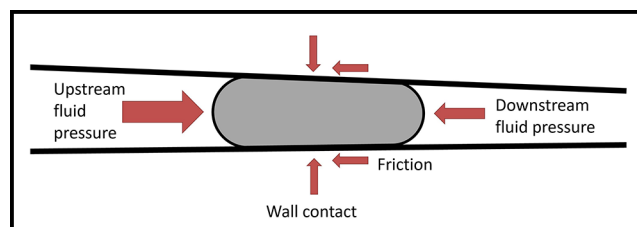

Figure 2: The bacteria cells experience mechanical loading in the tapered channels due to the fluid pressure, which varies from the upstream end to the downstream end.
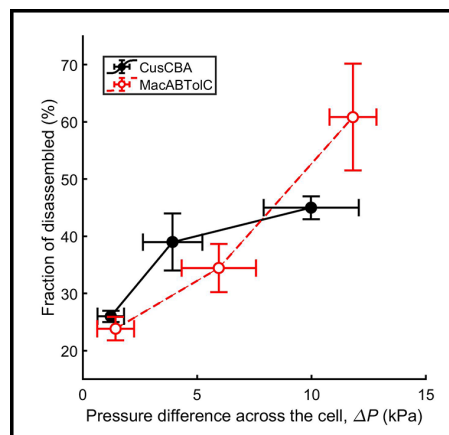
Figure 3: Increased mechanical loading (pressure difference across the cell), was shown to increase disassembly of the multicomponent efflux complexes CusCBA and MacABTolC in E. coli.
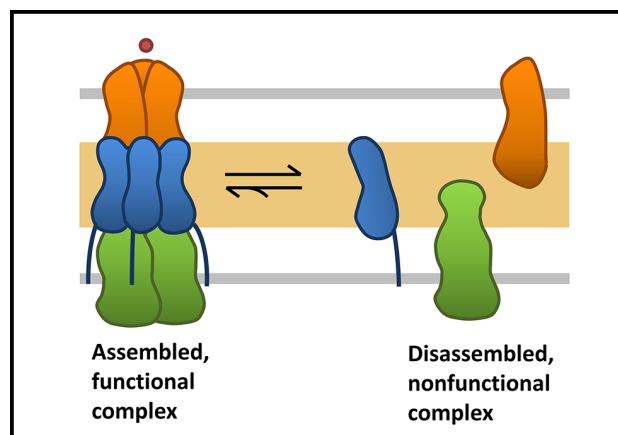

Figure 4: Multicomponent efflux complexes can be in an assembled and functional form or a disassembled and nonfunctional form. Disassembled complexes are unable to efflux toxins and antibiotics.

We manufacture our microfluidic devices on fused silica glass wafers using deep UV photolithography to achieve nano-scale features (250 nm smallest dimension). These glass-on-glass devices are manufactured using the AJA sputter deposition, ASML, PT770, Oxford 100, VersaLaser, and MOS clean anneal tools.

We are investigating the effects of mechanical stress and strain on two systems of antibiotic resistance found in bacteria: multicomponent efflux complexes and two component signal transduction systems. Multicomponent efflux complexes create channels that cross the cell envelope of bacteria and are used to pump toxins and antibiotics out of the cell. Our data suggests that the assembly and function of the multicomponent efflux complex CusCBA in *E. coli*, which effluxes the toxin copper, is impaired by increased mechanical loading (Figure 3) [2].

Preliminary evidence shows that other trans-envelope multicomponent complexes are also sensitive to the mechanical stress experienced by the cell. Disassembly of the multicomponent efflux complex MacABTolC, which effluxes macrolide antibiotics, also increases with the magnitude of mechanical loading (Figure 3) [3]. Disassembled CusCBA and MacABTolC complexes are nonfunctional and incapable exporting copper toxins and antibiotics, suggesting toxin and antibiotic resistance of mechanically stressed cells is reduced (Figure 4).

Two-component signal transduction systems are a key mechanism bacteria use to sense external stimuli and respond by altering gene expression. We are currently investigating a two-component system in *V. cholerae* that controls cell wall homeostasis and is essential for resistance to antibiotics that damage the cell wall. Preliminary work shows that this signaling pathway is activated by mechanical loading in our microfluidic device, providing exciting evidence that mechanical stimuli can affect gene expression in bacteria.

We are also working to better understand bacterial mechanical properties by combining experimental data from the microfluidic devices with finite element modelling to calculate numerical estimates for the Young's Modulus of the bacterial cell envelope. Establishing a reliable method of measuring the mechanical properties of the bacterial cell envelope will help us identify subcellular components that contribute to bacterial mechanics as well as how different environmental factors such as antibiotic treatment can change bacterial mechanical properties.

Conclusions and Future Steps:

So far our research has shown that mechanical stress and strain impairs the proper assembly and function of the cellular machinery needed for toxin and antibiotic efflux in *E. coli*. We also have preliminary evidence that a two-component system in *V. cholerae* regulates gene expression in response to mechanical stimuli.

In the future we will focus on using our microfluidic device to quantify the mechanical properties of different components of the bacterial cell envelope.

References:

[1] X. Sun, W.H. Weinlandt. H. Patel, M. Wu, C.J. Hernandez. (2014) "A Microfluidic Platform for Profiling Biomechanical Properties of Bacteria." Lab on a Chip. 14 (14), 2491-2498. NIHMS600175.

[2] L.A. Genova, M.F. Roberts, Y.C. Wong, C.E. Harper, A.G. Santiago, B. Fu, A. Srivastava, W. Jung, L.M Wang, Krzemiski, X. Mao, X. Sun, C.Y. Hui, P. Chen, C.J. Hernandez. (2019) "Mechanical stress compromises multicomponent efflux complexes in bacteria". Proc. of the National Academy of Sciences U. S. A. 116 (51) 25462-25467.

[3] C.E. Harper, W. Zhang, P. Chen, C.J. Hernandez. (2020) "Mechanical stress promotes disassembly of the antibiotic efflux complex MacAB-TolC". Biophysical Society AM. San Diego, CA, USA.

Design and Application of Microfluidic Devices to Study Cell Migration in Confined Environments

Abstract:

The ability of cells to migrate through tissues is an essential factor during development, tissue homeostasis, and immune cell mobility. At the same time, it enables cancer cells to invade surrounding tissues and metastasize. We have created microfluidic devices that mimic the narrow, heterogeneous interstitial spaces and that can be used to study nuclear mechanobiology during confined migration. Using these devices in combination with fluorescent imaging, we have developed a method to assess the confined migration fitness of varying cell types.

Research Summary:

During *in vivo* migration, cells such as immune cells, fibroblasts, or metastatic tumor cells traverse interstitial spaces as small as 1-2 μm in diameter. This 'confined migration' requires the deformation not only of the soft cell body but also the rate-limiting step of deforming the large (5-10 μm diameter) and relatively rigid nucleus [1]. To study these processes in more detail, we have previously designed and built polydimethylsiloxane (PDMS) microfluidic devices to model the tight three-dimensional constrictions that metastatic cancer cells may encounter during the metastatic process [2]. These devices support a wide range of cell lines and enable high-quality fluorescence imaging of nuclear lamina bucking, chromatin strain, DNA damage and nuclear rupture/blebbing and repair [2-4]. However, these devices require time-consuming single-cell analysis, do not fully mimic the heterogeneously confining nature of interstitial spaces, and do not allow use of sufficient cell numbers for biological and genomic analyses of cells that have migrated through the confined spaces due to their relatively small constriction areas (Figure 1).

Figure 1: Overview of cancer cell migration device. Top: Partial figure reproduced from Davidson, et al. [2]. Previous PDMS microfluidic devices bonded on glass coverslips and filled with food coloring dye. Bottom: New design of "random pillar" microfluidic devices also bonded to glass coverslip and filled with food coloring. CAD for constriction areas of each design shown (outlined in red on left). Scale bars: 30 μm. All devices have migration areas with 5 μm height. Figure adapted from manuscript submitted to Methods in Molecular Biology.

To overcome these limitations, we have designed novel migration devices that mimic the intermittent confinement of interstitial environments using a precisely controlled but heterogeneous "field of pillars" with variable spacing

Figure 2: Schematic overview of the PDMS migration device. Top and side view of the device after bonding to glass slide to create a confined environment for cancer cell migration (red area). Figure adapted from manuscript submitted to Methods in Molecular Biology.

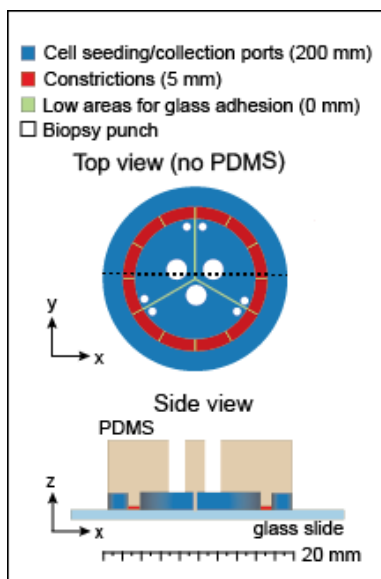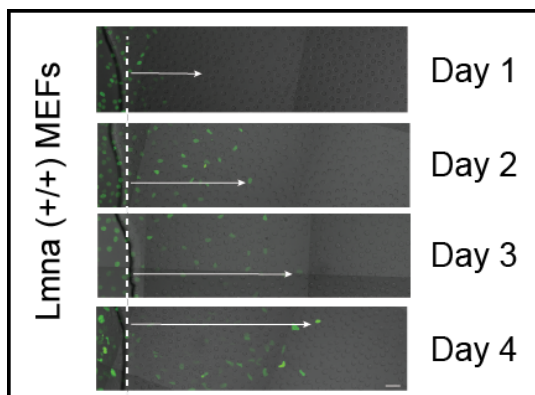*Figure 3: Cell migration in microfluidic device. Representative image series to show usage of microfluidic devices to determine migratory fitness as a function of distance traveled from seeding port into constriction area (white arrows) over four days. Figure adapted from manuscript submitted to Methods in Molecular Biology.*
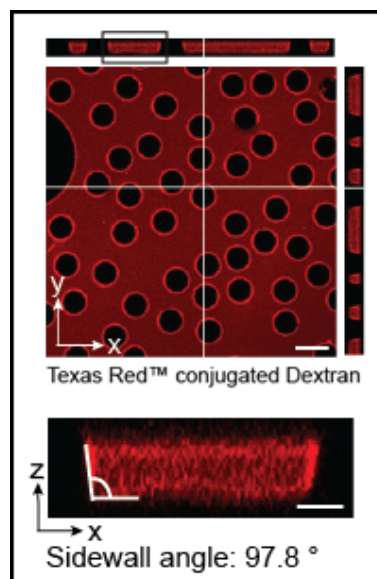

Figure 4: Confocal 3D reconstruction of confined migration area. The PDMS microfluidic device was bonded to a glass coverslip, filled with fluorescent TexasRed-conjugated Dextran, and imaged by confocal microscopy to create a 3D image stacks. Orthogonal projection used to measure sidewall angle, α, of 97.8°. Scale bars: 4 µm. Figure adapted from manuscript submitted to Methods in Molecular Biology.

(Figures 1 and 2). These new devices enable not only time-lapse microscopy, but also straightforward assessment of migratory fitness based on the distance traveled by the cells from the seeding port (Figure 3). These devices are also more amendable to enable collection of large numbers of cells following confined migration. Thus, the new devices present a high-throughput method for observing the short- and longer-term effects mechanically induced nuclear deformation and rupture has on the tumor cells.

In addition to the design, we have also improved the microfabrication methods of wafer used as the mold for the PDMS devices. Wafers for previous device generations were generated using either a thin layer of SU-8 photoresist or reactive ion etching (RIE) fabrication using the photonics etch in the Unaxis 770 deep silicon etcher. However, SU-8 lacked the fidelity to reproduce our fine features (1μm), and repeated molding and removal of PDMS would, over time, weaken the SU-8/silicon substrate bond, eventually resulting in the delaminating of features. RIE etching in the Unaxis 770 enabled us to create our desired features but required time-consuming seasoning and re-seasoning of the chamber before and after the long photonics etch, as it is traditionally a deep reactive ion etching (DRIE) tool.

For the new devices, we shifted the nanofabrication process to etching using hydrogen bromide in the Oxford Cobra etcher, which has proven to be a highly efficient, reliable method to achieve vertical sidewalls (Figure 4). This revised approach has a faster etch rate than our previous RIE process and enabled us to improve the fidelity of our critical features, while also reducing the fabrication time and costs by more than two thirds.

We highly recommend etching using hydrogen bromide for the creation of PDMS microfluidic devices.

Future fabrication efforts will be focused on transitioning this process to a stepper, as this will enable us to create "taller" constrictions to serve as a vertically "unconfined control" ($> 10 \mu$m), which cannot currently be performed using HBr etching. The stepper approach will also enable additional modularity for device layout on wafers and allow us to produce our submicron features with greater ease, instead of the current "trial-and-error" exposure arrays required for the contact lithography process. Taken together, these examples illustrate new uses of the available nanofabrication technologies to create improved *in vitro* models to study cancer cell migration.

References:

[1] Davidson, P. M., Denais, C., Bakshi, M. C., and Lammerding, J. Nuclear deformability constitutes a rate-limiting step during cell migration in 3-D environments. Cell. Mol. Bioeng. 7, 293-306 (2014).

[2] Davidson, P. M., Sliz, J., Isermann, P., Denais, C., and Lammerding, J. Design of a microfluidic device to quantify dynamic intra-nuclear deformation during cell migration through confining environments, Integrative Biology, Volume 7, Issue 12, December 2015, Pages 1534-1546, https://doi.org/10.1039/c5ib00200a.

[3] Shah, P., et al. Nuclear Deformation Causes DNA Damage by Increasing Replication Stress. Curr. Biol. 31, 753-765.e6 (2021).

[4] Denais, C. M. et al. Nuclear envelope rupture and repair during cancer cell migration. Science Vol. 352, Issue 6283, pp. 353-358 (2016).

Microfabrication of Fixed Length Sample Holders for Cryogenic Small Angle X-Ray Scattering

Abstract:

Small-angle X-ray scattering (SAXS) is a key tool for probing the structure and function of proteins, nucleic acids, and macromolecular complexes. Most synchrotron sources have dedicated BioSAXS beam lines, but efforts to improve their throughput have not kept pace with user demand. Large sample volumes and low duty cycles are critical bottlenecks in the expansion of BioSAXS. Cryogenic sample freezing overcame these bottlenecks in an analogous X-ray technique, macromolecular crystallography. Cryocooling significantly reduces the effects of X-ray radiation damage, reducing the necessary sample volume to collect adequate amounts of data, and eases the sample handling procedure of sensitive or unstable samples. Likewise, CryoSAXS should require much smaller sample volumes per measurement, allow sample preparation in the home lab immediately after purification, easy sample storage and shipping, and automated high-throughput data collection. This will enable dramatically more efficient use of both biomolecules and synchrotron beam time, and significantly expand the potential scope of BioSAXS studies.

Summary of Research:

We envision CryoSAXS as a routine method analogous to cryocooling in macromolecular crystallography (MX). The reduction in radiation damage at T = 100 K significantly reduces the amount of protein required per measurement and sample holders compatible with standard macromolecular cryocrystallography (MX) infrastructure could be transformative step in increasing the throughput and potential of BioSAXS. CryoSAXS could be especially useful for high-throughput parameter and ligand interaction screening, the study of difficult to produce proteins or complexes, and extremely radiation sensitive targets, applications in which BioSAXS may have the greatest impact on human health.

Despite the demonstrations of its potential [1,2], the lack of a robust experimental platform has prevented CryoSAXS from becoming a routine experimental technique. The need to subtract a highly matched background scattering pattern from the macromolecule's scatter and the difficulty in vitrifying bulk-like solutions have posed serious technical challenges for the development of sample holders adequate for routine use. Shown in Figure 1 is a new generation of CryoSAXS devices we recently developed using microfabrication techniques at the Cornell NanoScale Science and Technology Facility (CNF).

These devices constrain the sample held between two silicon nitride windows at a 1 mm fixed pathlength. Double-sided polished wafers coated in 500 nm of low-pressure chemical vapor deposition silicon nitride using
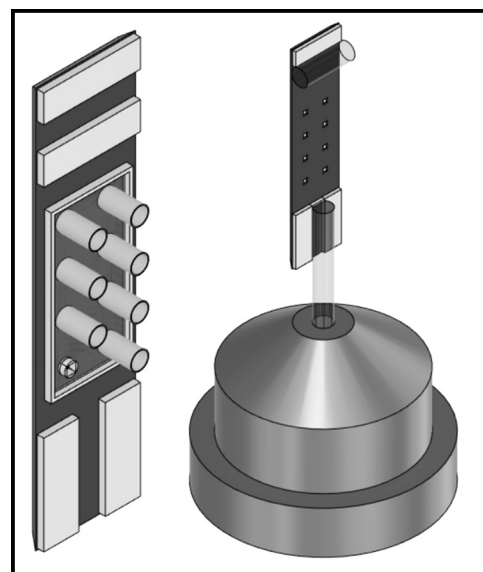

Figure 1: Images of CryoSAXS sample devices. The sample is held in place between two silicon nitride X-ray windows by Kapton® tube. The X-ray passes axially through the tubing. Multiple sample cells are present in a single device in two rows. One row contains solutions with a macromolecule and the other is analogous solutions without the macromolecule to be used for background subtraction.

the LPCVD CMOS nitride furnace (E4). Using the MA6-BA6 contact aligner, one side of the wafer was patterned with photoresist. The nitride was then dry etched with the Oxford 81 plasma etcher for a later potassium hydroxide (KOH) wet etch. SUEX was laminated onto the other side and patterned with backside alignment using the MA6-BA6 contact aligner. The SUEX features serve as guides for alignment and to help position tubes. A KOH wet etch then formed the X-ray windows and diced the wafer. The VersaLaser was used to cut spacers from 1 mm diameter quartz glass rods and affixed to one wafer pieces. Using jigs for cutting and alignment, 1 mm long Kapton® tubing was cut and glued to the devices. The devices are filled from the open end of the tube, then a second wafer piece is affixed to the top of the device to seal the sample. The samples are then cryogenically frozen in a cold nitrogen gas stream at T = 100 K for data collection.

X-ray data collection was performed at Cornell High Energy Synchrotron Source (CHESS) beamline ID7A and NSLS-II beamline 16ID for the protein apoferritin using 35% w/w propylene glycol as a cryoprotectant. Figure 2 shows results from apoferritin at several protein concentrations.

Figure 2: Background subtracted X-ray diffraction intensity from apoferritin at different concentrations.

References:

[1] Meisburger, S. P., et al., (2013) Biophys. J., 104, 227-236.

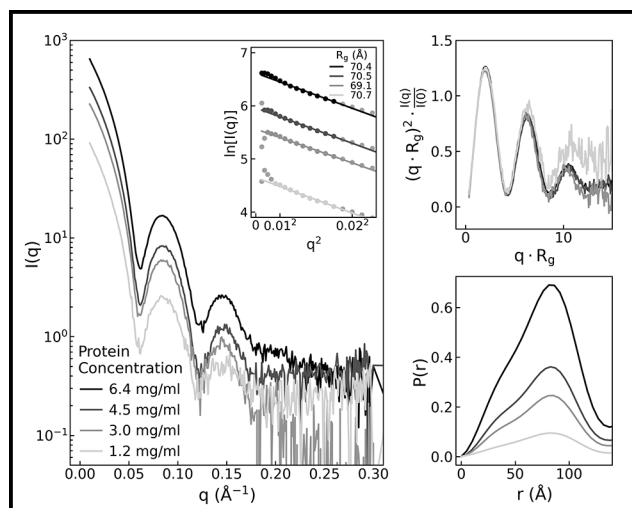[2] Hopkins, J. B., et al., (2015) J. Appl. Cryst. 48, 227-237.

Metasurface-Enhanced Infrared Spectroscopy for the Measurement of Live Cells

CNF Project Number: 2472-16

Principal Investigator(s): Gennady Shvets

User(s): Steven He Huang, Po-Ting Shen, Aditya Mahalanabish

Affiliation(s): Applied and Engineering Physics, Cornell University

Contact(s): gs656@cornell.edu, hh623@cornell.edu, ps944@cornell.edu, am2952@cornell.edu
Website: http://shvets.aep.cornell.edu

Primary CNF Tools Used: JEOL 9500, CVC SC4500 evaporator, Zeiss Supra SEM, PDMS casting station, Anatech resist strip, Oxford PECVD

Abstract:

Infrared (IR) spectroscopy for the label-free, nondestructive analysis of biological samples is a rapidly expanding area of research. We have developed Metasurface-Enhanced Infrared Spectroscopy (MEIRS) as a novel tool to perform spectral analysis of live cells in standard cell culture conditions. The cells are cultured on plasmonic nanoantennas (metasurface), and the plasmonic hotspots are used to enhance the IR signal. We have used MEIRS to track the spectral changes in the cells *in situ* as they are being treated with different chemical compounds. We are also investigating the effect of surface functionalization on the metasurface, with the aim of enhancing cellular signal by increasing the overlap between the cells and the infrared optical field.

Summary of Research:

Infrared (IR) spectroscopy is widely used to identify chemical compounds through their molecular vibration fingerprints and has recently found applications in the biological analysis as a tool for histology and cytopathology, identifying tumor tissues from normal tissues and monitoring the effect of chemotherapeutics on cancer cells. We have developed a novel technique called Metasurface-Enhanced Infrared Spectroscopy (MEIRS) to measure live cells in physiological conditions. In MEIRS, cells are seeded on a planar array of gold plasmonic nanoantennas called metasurfaces. These resonant nano-antennas support plasmonic hot spots in their vicinity, enhancing the light-matter interaction and IR absorption. In the past, we have used MEIRS to detect spectroscopic changes in response to cellular dissociation and cholesterol depletion [1]. Our current work focuses on further extending the application of this technique to the measurement of cellular response from chemotherapeutics, as well as exploring different chemical functionalization to improve the sensing capability of the device.

The plasmonic metasurfaces are fabricated in the CNF cleanroom. Metasurfaces are fabricated on IR-transparent CaF_2 substrates. First, patterns are defined on poly(methyl methacrylate) (PMMA) using electron beam lithography with the JEOL 9500 system. This is followed by gold evaporation and lift-off in acetone to create the gold nanoantennas. Once the fabrication is done, Anatech resist strip is used to clean the metasurface and remove any resist residues. To perform *in situ* spectroscopy with live cells, we use a polydimethylsiloxane (PDMS) based flow chamber to
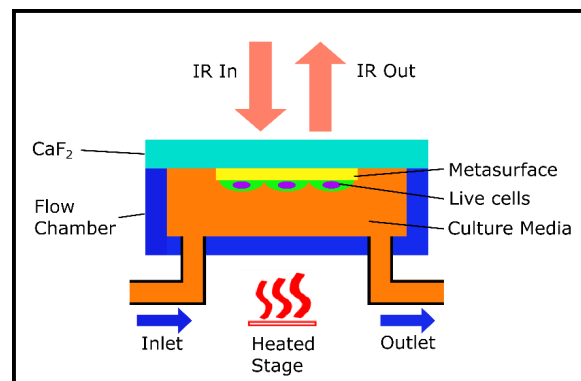

Figure 1: Schematic drawing of the flow-chamber setup for in situ *IR spectroscopy of live cells.*
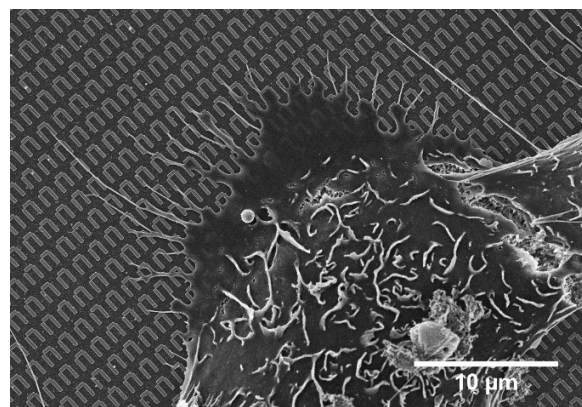

Figure 2: SEM of A431 cells grown on the plasmonic metasurface.

maintain physiological conditions, which is also fabricated at the CNF. A schematic drawing of our measurement setup is shown in Figure 1. We use human squamous carcinoma cell line A431 cells as a model system to investigate the cellular response. Scanning electron microscope (SEM) images of the cells on the metasurface (Figure 2) shows that the cells preferentially attach to the gold nanostructures rather than the CaF_2 substrate.

Using MEIRS, we have investigated the action of tricarbonyl rhenium isonitrile polypyridyl (TRIP) complex [2], a novel chemotherapeutic developed by our collaborator (Wilson group, Cornell University), on A431 cells. TRIP has been previously shown to induced endoplasmic reticulum (ER) stress that eventually leads to apoptosis. Figure 3 shows the detection of protein absorbance signal with MEIRS in real-time while the cells are being treated by TRIP at different concentrations. The control group showed a slight increase in protein signal, while TRIP-treated cells showed clear reduction in protein signal. The protein signal reduction is larger for a higher dosage of TRIP and this is in line with what we expect, given that TRIP can induce unfolded protein response through ER stress.

To improve the sensitivity of the metasurface we use chemical functionalization to achieve cell blocking on the IR transparent substrate while enhancing their attachment to the metallic antennas. The interaction between the evanescent fields of the metasurface and the cells depends
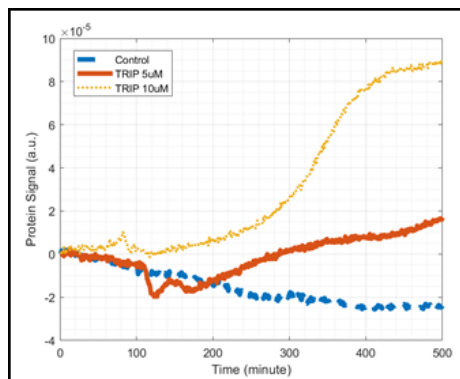

Figure 3: Protein signal from A431 cells in response to TRIP treatment. Infrared spectra collected in real-time are analyzed with principal component analysis (PCA). The spectral features at amide I and amide II absorption peaks are captured by the first principal component, the score from which is shown as the protein signal. The +y direction corresponds to a decrease in protein signal from cells.

principally on the placement of their focal adhesion on the metasurface. This functionalization process aims to increase the overlap of the cells with the metasurface hotspot, due to which we expect a significant increase in the spectroscopic intensity.

To controllably block cell adhesion on the CaF_2 substrate, it is first coated with a thin layer of silica (~100 nm) using the Oxford PECVD tool, followed by deposition of a self-assembled monolayer of silane conjugated polyethylene glycol (PEG) [3]. The gold nano-antennas are functionalized using n-alkanethiols [3]. This ensures the cells preferentially attach to the nanoantennas. Figure 4 (left) shows A431 cell attachment on an un-functionalized metasurface. We can see how the cells cover the metasurface as well as the substrate. Figure 4 (right) shows A431 cell attachment after the metasurface was functionalized. We can see the cells cover only the metasurface area and are blocked from the substrate region.

References:

[1] S. H. Huang, J. Li, Z. Fan, R. Delgado and G. Shvets. bioRxiv 2021.06.30.450584.

[2] A. P. King, S. C. Marker, R. V. Swanda, J. J. Woods, S. B. Qian and J. J. Wilson, Chem. - A Eur. J., 2019, 25, 9206-9210.

[3] S. Lan, M. Veiseh and M. Zhang, Biosens. Bioelectron., 2005, 20, 1697-1708.
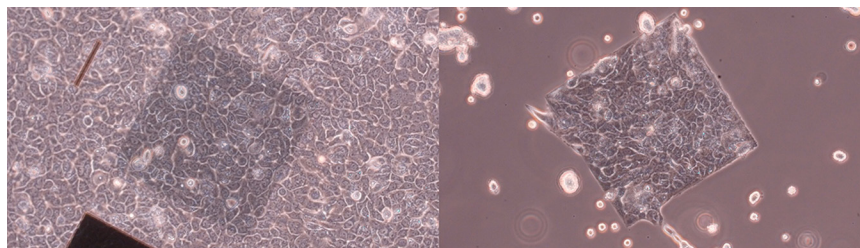

Figure 4: (left) A431 cell attachment on an unfunctionalized metasurface sample. (right) A431 cell attachment on metasurface sample after functionalization.

Retinal Implant Project

CNF Project Number: 2504-16

Principal Investigator(s): Douglas Shire, Ph.D.[1,2,3]

User(s): Marcus Gingerich, Ph.D.[1,3]

Affiliation(s): 1. Department of Electrical Engineering, Cornell University; 2. VA Cleveland Healthcare System; 3. Bionic Eye Technologies, Inc.

Primary Source(s) of Research Funding: NIH R43 NS113708-01

Contact(s): dbs6@cornell.edu, mdg37@cornell.edu

Website: http://www.bostonretinalimplant.org

Primary CNF Tools Used: PT-72, lithography toolset/MA6, Heidelberg mask writer - DWL2000, evaporators, AJA sputter deposition, SEMs, gold electro-plating, Class 2 lithography toolset, Oxford PECVD, Oxford 100 etcher, Oxford Cobra etcher, Glenn 1000, YES polyimide oven, Parylene-C coater, VersaLaser, numerous metrology tools

Abstract:

The purpose of the Retinal Implant Project is to restore useful vision to patients who are blind with degenerative retinal diseases. The primary illnesses we hope to treat are retinitis pigmentosa (a primary cause of inherited blindness) and age-related macular degeneration (the leading cause of blindness in the developed world). Both these diseases cause the eventual destruction of the photoreceptor cells — rods and cones — in the retina, leaving intact the ganglion cells that transmit electrical impulses (and hence visual information) to the brain. The ganglion cells may be stimulated, however, with biphasic current pulses from a microfabricated electrode array. Blind surgical volunteers have consistently described visual percepts that resulted from such stimuli, and this has led our team to develop a wireless, implantable retinal prosthesis. More recently, we have also begun work on developing a system which can induce visual percepts deeper in the brain into the lateral geniculate nucleus.

Summary of Research:

The implanted portion of our device consists of power and data secondary receiving coils, and — in a sealed titanium (Ti) can — a small number of discrete components, and a custom designed application specific integrated circuit (ASIC), which consists of circuitry for clock and data recovery, current drivers for electrodes in a stimulating electrode array, and a programmable function generator capable of stimulating with a wide range of pulse widths and amplitudes. The current outputs drive high-charge capacity sputtered iridium oxide film (SIROF) stimulating electrodes, which in turn give rise to the visual percepts mentioned above.

CNF-fabricated components of this system have included various proof-of-concept test structures and tools used in the research effort and an integrated combination flexible circuit and stimulating electrode array. Silicon (Si) wafers serve as carriers for these freestanding films during processing. The electrode leads are fabricated inside of 'sandwiches' of polyimide and amorphous silicon carbide (SiC), while the SIROF electrodes are reactively sputter-deposited.

Assembly of the intraocular components of the prosthesis is accomplished by flip chip solder ball bonding of the IC and solder attachment of discrete components onto an internal flexible circuit board, which is hermetically sealed into an ultraminiature Ti can. The RF coils are soldered and glued to the integrated external flex-array which is in turn thermosonically bonded to the hermetic feedthrough of the Ti can. Finally, the thermosonic bonds are protected and insulated with an over-mold. An external patient interface unit, will consist of a video camera for capturing images, a digital signal processor, and a radio frequency (RF) transmitter and coil to relay power and data to the implanted device.

Scientific challenges still remain in realizing a chronically implantable retinal prosthesis. While our first-generation device was primarily encapsulated in polymers for short term proof-of-concept implant studies, our second-generation system focused on a system which would last many years *in vivo*. Our past efforts have focused on developing a device with 256+ stimulation channels that is still small enough and of a configuration to be easily implanted in the ocular orbit and continue to function for many years *in vivo*. Thus, a major effort has been the development of a technological platform to build a robust, hermetically packaged, high-density subretinal visual prosthesis with a lifetime of > 10 years in biological saline that is scalable to hundreds of I/O channels.
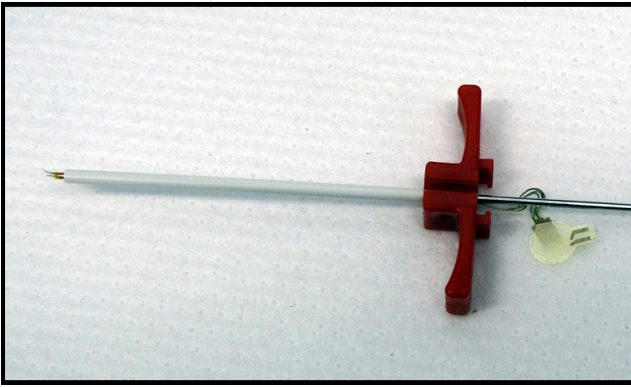
Figure 1: A prototype deep brain insertion sub-assembly is shown which includes a protective split-sheath inserter, the actual electrode array/ signal cable and the tungsten insertion rod.
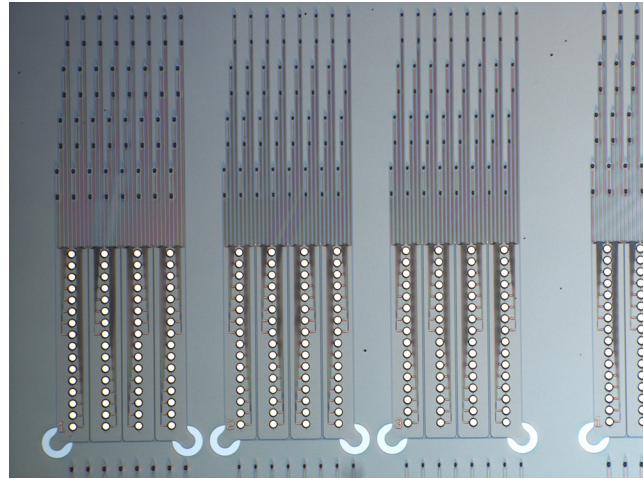

Figure 2: An optical image of three versions of test arrays, which each have four tine lengths and two electrodes per tine.
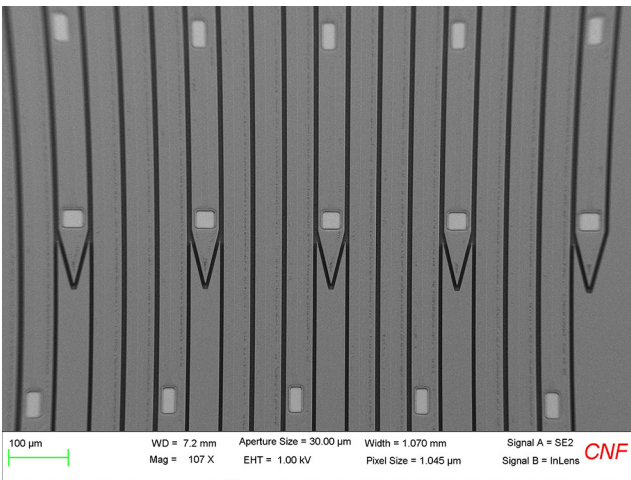

Figure 3: An SEM showing some of the tines just after the outline etching step, but while still on the Si carrier wafer.
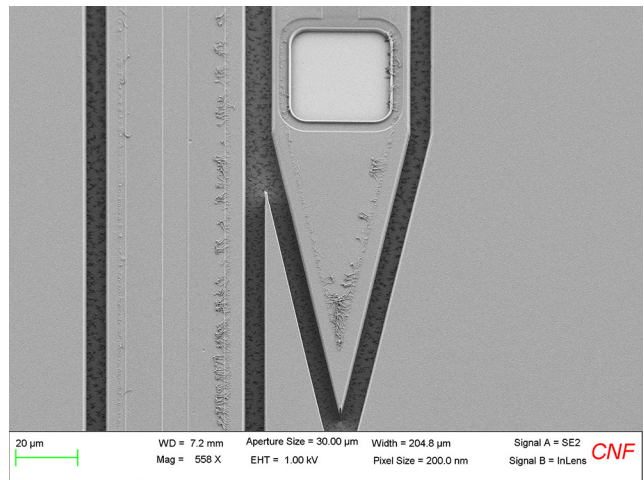

Figure 4: An SEM image of the electrode near the tip of a tine.

Recent efforts at the CNF have turned to developing a microfabrication process for penetrating electrodes for long-term implantation in brain tissue. The goal is to extend the existing retinal stimulator platform to include electrodes which can be placed at different points in the visual tract to enable the restoration of sight due to other causes of blindness. These electrodes can be placed into structures such as the lateral geniculate nucleus (LGN) to produce visual signals at that location. The LGN is a structure located deeper within the brain thus a system of implanting the electrode array into the target location has had to be developed as well.

An early prototype insertion device, shown in Figure 1, includes a protective split-sheath inserter, the actual electrode array/signal cable and the insertion rod. The resulting system has the potential to be utilized in other applications such as those requiring deep brain stimulation including Parkinson's disease, severe depression, morbid obesity, and obsessive-compulsive disorder, to name a few.

Long-term compatible LGN electrodes have been fabricated on a Si carrier wafer using an initial polyimide layer followed by a 2 μm-thick layer of PECVD SiC above and below a metal conductor layer with SIROF electrodes as the electrode/tissue interface material. The devices are shown post-outline-etch in Figures 2-4.

References:

[1] J. F. Rizzo, J. Wyatt, J. Loewenstein, S. Kelly, and D. Shire, "Methods and Perceptual Thresholds for Short-Term Electrical Stimulation of Human Retina with Microelectrode Arrays," Investigative Ophthalmology and Visual Science, vol. 44, no. 12, Dec. 2003, pp. 5355-5361.

Development of Heparin-Based Coacervate Loaded Liposomes as Non-Invasive Therapy for Myocardial Infarction

CNF Project Number: 2754-18

Principal Investigator(s): Yadong Wang

User(s): Chia-Wei Yeh

Affiliation(s): Biomedical Engineering, Cornell University
Primary Source(s) of Research Funding: Cornell Startup Funds
Contact(s): yw839@cornell.edu, cy465@cornell.edu
Primary CNF Tools Used: Heidelberg mask writer - DWL2000, ABM contact aligner, Zetasizer Nano-ZS

Abstract:

Cardiovascular disease is one of the major leading causes of death worldwide. Specifically, myocardial infarction (MI), generally known as heart attack, is the main cause of death in cardiovascular disease. Among them, the major cause of death of MI is due to myocyte necrosis and heart failure. The acute inflammation after MI may be resolved by draining the excessive tissue fluid through lymphatic networks around the heart. However, the high interstitial pressure in the infarcted area may impede the drainage, and the newly formed lymphatic networks due to the MI are not functional. Thus, unresolved inflammation may further exacerbate the damage to the heart tissue.

Vascular endothelial growth factor type C (VEGF-C) is known for inducing lymphangiogenesis both *in vitro* and *in vivo*. Several studies reported that by administrating VEGF-C after MI on rat model can effectively resolve the acute inflammation, and furthermore improve the cardiac function. Therefore, it is of particular promise to deliver VEGF-C to the infarcted heart area, induce lymphangiogenesis, resolve the acute inflammation after MI as well as facilitate injured heart tissue to regenerate.

Summary of Research:

Coacervate is an electrostatically bound complex between cationic and anionic polyelectrolytes. In the extracellular matrix (ECM), glycosaminoglycan such as heparan sulfate proteoglycan (HSPG) binds with several growth factors (GFs) to form HSPG-GF complex. This complex not only serves as reservoir for bonding and stabilization of GFs but also potentiates GFs responsible for maintaining normal cellular function. Due to the similar mechanism of protein-extracellular matrix interaction, it has been shown that heparin-based coacervate is a promising candidate for protein delivery system in biomedical and tissue engineering applications. Nevertheless, coacervate complex is unstable in the blood stream owing to the relatively weak electrostatic interaction within coacervate droplets, leading to the difficulty to systemically administer coacervate via intravenous injection.

In this study, we aim to develop a liposome filled with heparin based coacervate, namely lipocoacervate in short, for protein delivery to treat MI. Polyanion heparin is utilized to complex with vascular endothelial growth factors

C (VEGF-C) to form heparin-growth factor complex, which is then mixed with synthetic polycation, ploy(ethylene arginyl aspartate diglyceride) (PEAD) to construct VEGF-C loaded coacervate droplets. Also, staggered herringbone micromixer (SHM) microfluidics is designed to generate lipid vesicles. The VEGF-C loaded coacervate will then be mixed with the lipid vesicles to form lipocoacervate. The therapeutic effect of the lipocoacervate will be evaluated on rat myocardial infarction model.

Research Steps:

The negatively charged lipid vesicles were prepared by mixing DOPC/DSPG/cholesterol (molar ratio = 5/1/3) ethanol solution with 0.9% saline in SHM chip. The flow rate ratio between ethanolic and aqueous phase is 5, resulting negatively charged lipid vesicles (zeta potential = -3.11 ± 0.49 mV) with 70 nm in diameter. In order to facilitate the negatively charged lipid vesicles assemble onto coacervate, different PEAD to heparin (P/H) ratio was tested to figure
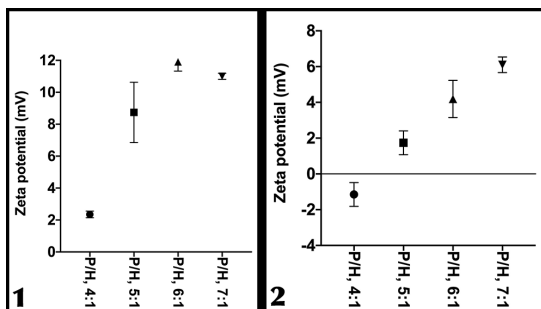
Figure 1, left: Zeta potential of PEAD/heparin coacervate before adding negatively charged lipid vesicles vs. P/H ratio. Figure 2, right: Zeta potential of lipocoacervate vs. P/H ratio.
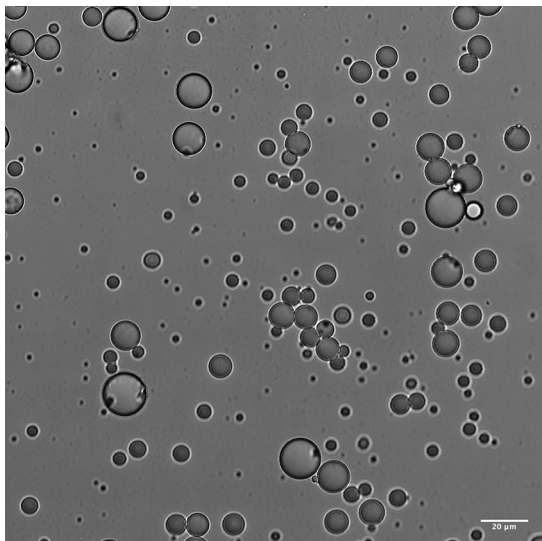
out the zeta potential of coacervate, as shown in Figure 1. As the P/H ratio increased, the zeta potential also increased. When the negatively charged lipid vesicles were mixed with coacervate, the zeta potential was reduced due to the electrostatic adsorption of the negatively charged lipid vesicles on coacervate, as shown in Figure 2. For visualizing the structure of lipocoacervate, rhodamine labeled PE (red) was added into lipid solution during the preparation of lipidvesicles, and fluorescein labeled bovine serum albumin (green) was also incorporated into PEAD/heparin coacervate for visualization.

The confocal images in Figure 3 and Figure 4 showed that the red lipid was indeed outside of green coacervate core, suggesting the successfully assembly of lipocoacervate.

Future works will be focused on investigating the lipid structure outside of coacervate, testing the stability of lipocaocervate, and evaluating the lymphangiogesis efficacy of VEGF-C loaded lipocoacervate.

Figure 3: Confocal image of lipocoacervate, bright field. Scale bar, 20 µm.

References:

[1] Hamano, N., et al. "Robust Microfluidic Technology and New Lipid Composition for Fabrication of Curcumin-Loaded Liposome: Effect on the Anticancer Activity and Safety of Cisplatin." Molecular Pharmaceutics 2019, 16, 3957-3967.

[2] Cakmak, F., et al. "Lipid Vesicle-Coated Complex Coacervates." Langmuir 2019, 35, 7830-7840.

[3] Zang, Y., et al. "Giant Coacervate Vesicles as an Integrated Approach to Cytomimetic Modeling." JACS 2021, 143, 2866-2874.
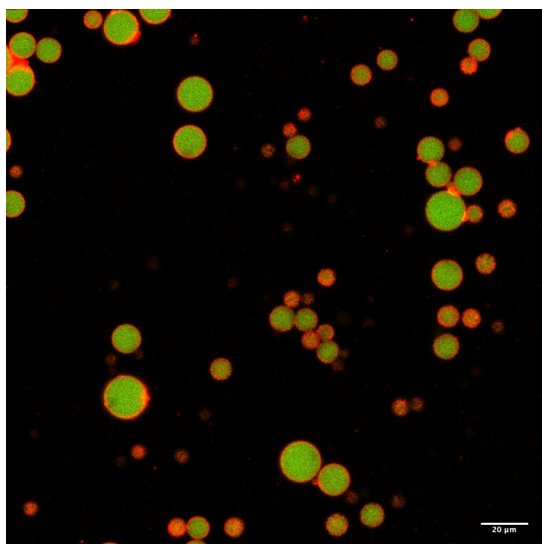
Figure 4: Confocal image of lipocoacervate, red: rhodamine labeled PE; green: fluorescein labeled BSA. The red lipid outside of green coacervate core suggesting the successful assembly of lipocoacervate. Scale bar, 20 µm.

Test Chip for Impedance Spectroscopy of Neuro Excitability

CNF Project Number: 2832-19

Principal Investigator(s): Prof. Huili Grace Xing

User(s): Mohammad Javad Asadi

Affiliation(s): School of Electrical and Computer Engineering, Cornell University
Primary Source(s) of Research Funding: Air Force Office of Scientific Research
Contact(s): grace.xing@cornell.edu, ma2297@cornell.edu
Primary CNF Tools Used: ABM contact aligner, SÜSS MA6-BA6 contact aligner, GCA AutoStep 200 DSW i-line wafer stepper,
Heidelberg mask writer, Glen 1000 resist strip, CVC SC4500 odd-hour evaporator, Zeiss Supra SEM

Abstract:

This report focuses on the efforts for fabrication of a test chip containing coplanar waveguides and designed for impedance spectroscopy of neuron excitability. Since there has been a mysterious problem during the fabrication of the chip, we elaborate on the efforts to find the root cause of this issue. Finally, some conclusions will be provided along with suggestions to be tried to alleviate the problem.
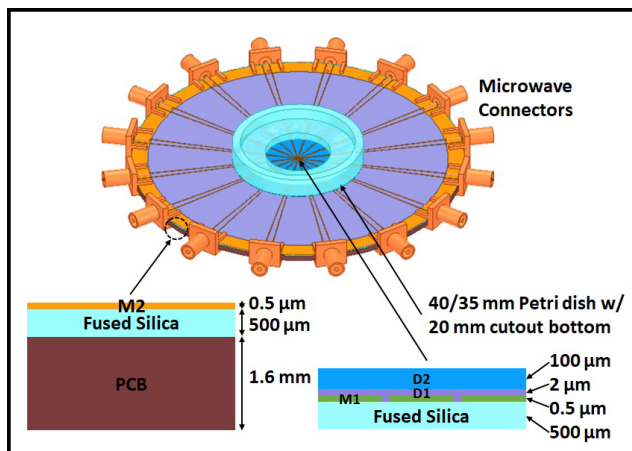
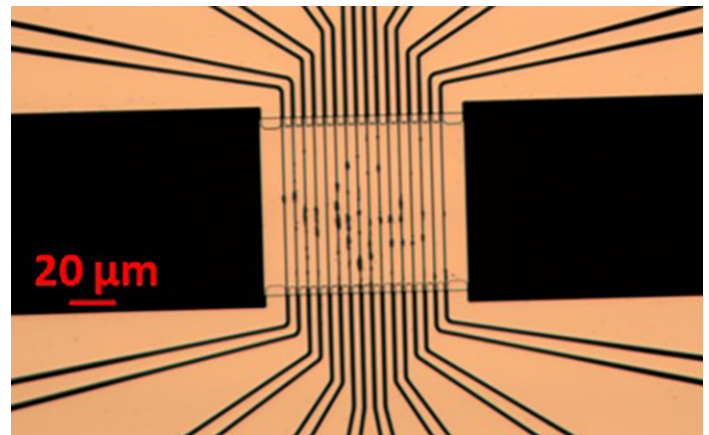*Figure 1: Top view of the designed test chip mated with a Petri® dish.*

Figure 2: Micrograph of the gold M1 and M2 fabricated on a fused silica wafer.

Summary of Research:

Figure 1 shows the designed test chip. It can be seen that the chip serves as the bottom of a Petri® dish reservoir through a 20-mm-diameter cutout in the bottom of the Petri dish. The chip comprises eight coplanar waveguides (CPWs) fabricated on a 0.5-mm-thick, 100-mm-diameter fused silica wafer. Sixteen microwave connectors of sub-miniature type A (SMA) are attached on the edge of the fused silica wafer in a radial pattern. The fused silica wafer is mechanically strengthened by a 1.6-mm-thick FR4 printed circuit board (PCB) with a 40-mm cutout to allow transmission optical microscopy of the center portion of the fused silica wafer. A microfluidic channel (100 μm long, 20 μm wide, 2 μm high) for axons is formed on the fused silica wafer with 2-μm-thick SU-8 walls and a 100-μm-thick polydimethylsiloxane (PDMS) cover. To electrically insulate the CPWs from the

culture medium outside the microfluidic channel, the SU-8 covers most of the fused silica wafer and the PDMS covers most the cutout of the bottom of the Petri dish.

The fabrication process for the entire chip is a four-mask process. The first two layers that were fabricated are metal 1 (M1) at the center of the chip, and metal 2 (M2) for the rest. The photolithography for M1 was done using the GCA AutoStep 200 DSW i-line wafer stepper to create a pattern with gaps of 1 μm. CVC SC4500 odd-hour evaporator was used to deposit 15 nm and 200 nm of titanium and gold, respectively, as M1. The same process but using SÜSS MA6-BA6 contact aligner was done to deposit 15 nm and 500 nm of titanium and gold respectively, as M2. The fabricated two metal layers is shown in Figure 2.

As can be seen in the figure, once M2 is deposited, and lift-off process is done, the M1 starts to develop some mouse bites. However, this kind of defects never observed in M1 before M2 is deposited and lifted off.

As a scanning electron microscopy (SEM) image of the M1, shown in Figure 3 confirms, the metal is severely damaged after fabrication. In order to solve this problem, several suggestions were tried such as not using RCA cleaning, not sonication for lift off, using brand new crucibles and metal sources for evaporation, and prebaking the wafers for several days before fabrication. However, none of these suggestions were helpful.

Successful fabrication without any mouse bite on a silicon wafer instead of fused silica led us to come up with a hypothesis that the problem is due to the electrostatic discharging effect.

In order to verify this hypothesis, half of the coplanar waveguide lines fabricated using aluminum were shorted while kept the rest intact. The result is shown in Figure 4.

As can be seen, the metal lines that are shorted and cannot build up static charge, are not damaged while the others developed mouse bite although not as severe as the case fabricated with gold. This test validates the assumption that the defects (mouse bites) are due to the electrostatic discharging that happens between each two isolated electrodes.

Conclusions and Future Steps:

We successfully found the root cause of the mouse bites that developed in the metal layer fabricated on a fused silica wafer. In the future, the isolated metal layers will be temporarily shorted up to the last fabrication step to make sure electrostatic discharging will not happen. Besides that, the fabricated metal layers will be covered with a thin layer of oxide that might help to mitigate the electrostatic discharging effect.
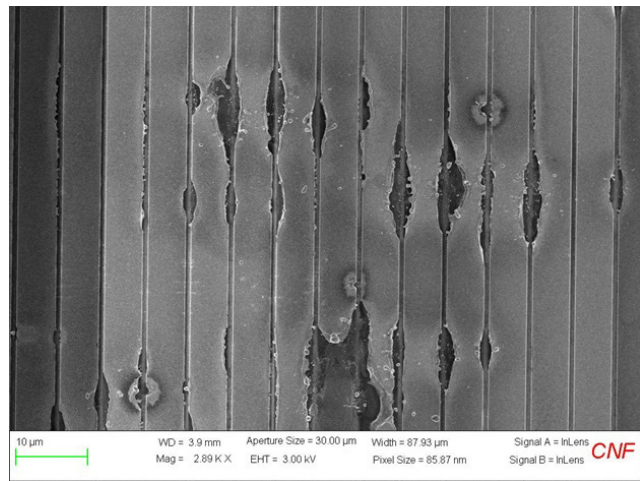
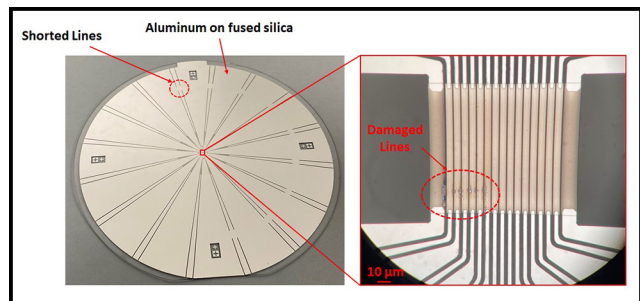*Figure 3: SEM image of the mouse bites in M1.*

Figure 4: Micrograph of the aluminum M1 and M2 fabricated on fused silica wafer.

Fabrication of Microchip Devices for Organ-on-a-Chip and Lab-on-a-Chip

CNF Project Number: 2857-19

Principal Investigator(s): Esak (Isaac) Lee, Ph.D.

User(s): Renhao Lu

Abstract:

Triple-negative breast cancer (TNBC) is one of the most insidious forms of breast cancer. Among multiple metastatic processes, extravasation determines the final site of the metastasis. We developed a rapid multilayer microfabrication method of transferring a three-dimensional (3D) overhang pattern to a substrate with a sacrificial layer to reconstitute a 3D blood vessel surrounded by the extracellular matrix containing organ-specific parenchymal cells. Based on our *in vitro* model, we found that bone-like microenviroment with osteoblasts and mesenchymal stem cells promoted extravasation of the bone-tropic TNBC cells, whereas the lung-like microenviroment promoted extravasation of the lung-tropic TNBC cells.

Summary of Research:

Despite numerous research efforts, triple-negative breast cancer (TNBC) is the most aggressive form of breast cancer and still the leading cause of cancer deaths in breast cancer patients. Physicians have discovered that breast cancer highly prefers to certain organs for metastases [1], referring as organotropic cancer metastasis. To better understand and treat TNBC metastasis, we need to look into TNBC interactions with blood vessels through bio-mimic models.

Needle-based casting method has been used as a conventional tool for fabricating engineered vessels with an ease of obtaining a cylindrical shape in 3D matrices [2]. However, a needle buffer layer has to be prepared, and additionally mix of photo resist is required to produce a blocking layer [2], which significantly harms the purity of the materials and weakens the bonding strength between the layers, thereby deteriorating the durability of the mold.

Here, we developed a novel microfabrication method allows the fabrication of a vascular channel with only single casting mold by transferring a 3D overhang two-layer SU-8 pattern to a substrate with a sacrificial layer. The casting mold with a 3D overhang pattern provides a more reproducible, reliable vascular conduit structure than previous methods described above.

The microfluidic vascular channel device design is shown in Figure 1(a). The device contains a circular inlet and outlet, an extracellular matrix (ECM) hydrogel cavity located in the center, and two ports to access the vessel lumens. The design is made using L-edit computer-aided design

software, and the ultraviolet (UV) photomasks for three layers are engraved on 5-inch-chromium masks by a laser pattern generator (Heidelberg mask writer - DWL2000).

Our PDMS microfluidic chip was fabricated using a conventional polydimethylsiloxane (PDMS) casting process. The microfabrication photolithography for PDMS mold began with two 100 mm silicon wafer substrates, one was used as a 'pattern wafer' (Figures 1(b) and (c)), and another was used as a 'mold wafer' (Figure 1(d)). For the pattern layer, firstly, a layer of OmniCoat™ was spin-coated on the whole surface. Next, a 450 μm thick layer of SU-8 2150 for a 100 μm thick gel-top layer and a 350 μm thick needle guide layer was spin-coated and soft-baked. This layer was exposed by two different masks (needle guide layer mask and gel-top layer mask) using ABM manual mask aligner.

After post-exposure baking (PEB) and cooling down, a 100 μm thick layer of SU-8 100 for the needle buffer layer was spin-coated, soft-baked and exposed. Simultaneously, on the mold wafer, a 50 μm thick layer of SU-8 50 for the bonding layer was spin-coated, soft-baked, and flood-exposed with 450 mJ cm^{-2} of UV exposure without a mask (Figure 1(d)).

Consequently, the two wafers were joined together facing each other, and we performed PEB and developed them together (Figure 1(e)). After the development, the wafers were further developed in an alkaline developer MF319 to remove the OmniCoat™ sacrificial layer, completing

the transferring process. The surface of the fabricated mold wafer was treated by a monolayer of FOTS through the molecular vapor deposition system (MVD 100).

Based on our PDMS microfluidic chip, we investigated breast tumor extravasation in distinct organs to recapitulate the critical step in the organotropic metastasis. Our study showed that bone-like microenviroment with osteoblasts and mesenchymal stem cells promoted extravasation of the bone-tropic TNBC cells, whereas the lung-like microenviroment promoted extravasation of the lung-tropic TNBC cells (Figure 2). Given that these organ-specific parenchymal cells do not impact vascular permeability, our results suggest that the parenchymal cells dictate selective extravasation of the bone-tropic or lung-tropic TNBC cells in our system.

Conclusions and Future Steps:

By transferring multilayer pattern to another wafer, we have achieved building SU-8 overhanging structure without any blocking layers. Furthermore, we found the tissue specific TNBS extravasation phenomenon based on our microfluidic chips.

In the future, we plan to dig into the biological mechanisms behind our findings. Also, we hope to expand our microfabrication chip into other biological applications, including lymphatic and glaucoma organ-on-a-chip models.

References:

[1] Patanaphan, V. I. N. I. T. A., Omar M. Salazar, and Rapael Risco. "Breast cancer: metastatic patterns and their prognosis." Southern medical journal 81.9 (1988): 1109-1112.

[2] Polacheck, William J., et al. "Microfabricated blood vessels for modeling the vascular transport barrier." Nature protocols 14.5 (2019): 1425-1454.

[3] Kwak, Tae Joon, and Esak Lee. "Rapid multilayer microfabrication for modeling organotropic metastasis in breast cancer." Biofabrication 13.1 (2020): 015002.
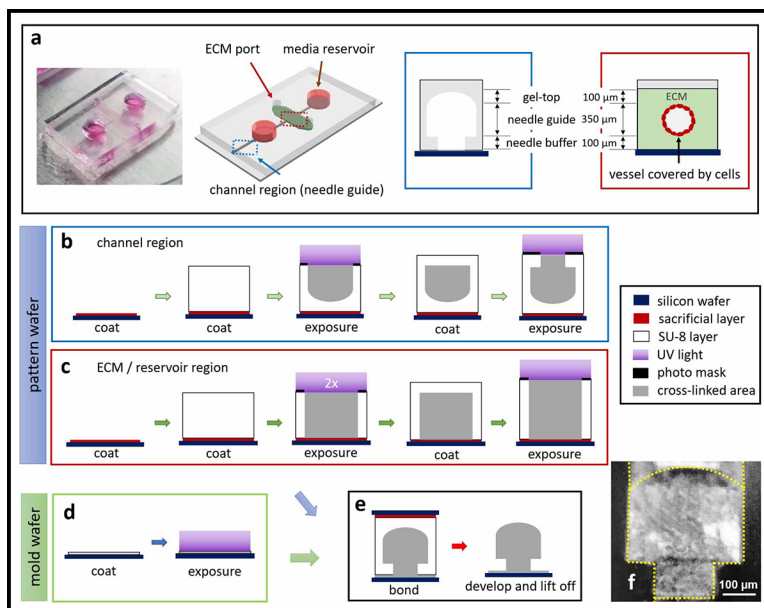
Figure 1: A schematic illustration of the rapid multilayer microfabrication method. (a) A real image of the device and an isometric illustration of the device (left); and in the right, there are cross-section views of the channel region (blue box) and the ECM hydrogel region (red box). (b)-(e) A multi-layer mold fabrication process for the channel region (b) and ECM /reservoir region (c) on the pattern wafer. (d) A flood-exposure is used to form a SU-8 bonding layer on the mold wafer. (e) The two wafers are bonded together by facing during a post-exposure bake (PEB) process and are developed to remove non-crosslinked SU-8 and the sacrificial layer. (f) A cross-section image of a multi-layered overhang structure in the channel region.
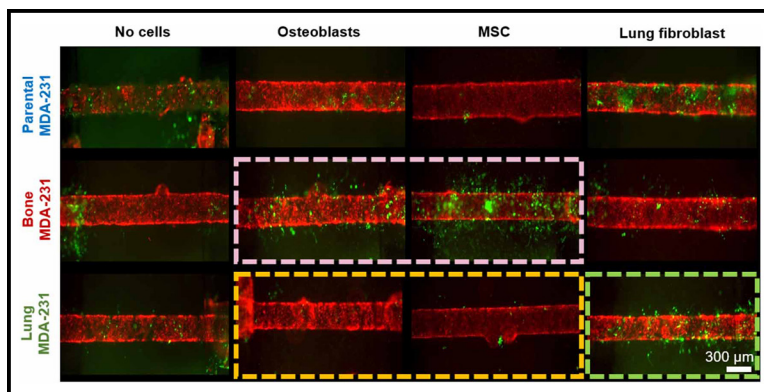

Figure 2: Organ-specific tumor metastasis 3D in vitro. Parental, bone-tropic, and lung-tropic MDA-MB-231 cells were introduced into blood vessels surrounded by collagen I with no cells, osteoblasts, bone-marrow derived MSC, and lung fibroblasts. The experiment was maintained for six days. Representative images at Day 6 are presented. The highlighted boxes (pink, orange, green) indicate the organ-specific extravasations.

Human MSCs Release Multiple EV Populations Containing Mitochondria

CNF Project Number: 2864-20

Principal Investigator(s): Dr. Michelle L. Delco, DVM, Ph.D., DACVS

User(s): Matthew Thomas

Affiliation(s): College of Veterinary Medicine, Department of Clinical Sciences; Cornell University

Contact(s): mld12@cornell.edu, mt826@cornell.edu
Primary CNF Tools Used: Malvern Nano ZS Zetasizer, Malvern NS300 NanoSight

Abstract:

A growing body of evidence supports intracellular mitochondrial (MT) transfer as an important intercellular signaling mechanism. Further, increasing evidence suggests that mesenchymal stromal cells (MSCs) can rescue injured and dysfunctional cells by donating whole mitochondria, and this phenomenon may explain the beneficial effects of therapeutically implanted MSCs. One possible mechanism for MT transfer involves packaging mitochondria into extracellular vesicles (EVs). This would open the possibility of cell-free MT-targeted regenerative therapies. Confirming that this is possible would be an important step toward therapeutic development. As demonstrated here, human MSCs produce EVs containing MT. We have used the CNF to further characterize these 'mitovesicles' and found that there are multiple populations of different sizes, indicating different modes of biogenesis and/or distinct bio-signaling functions.

Summary of Research:

The phenomenon of intercellular mitochondrial transfer, by which mesenchymal stromal cells donate whole mito-chondria (MT) to other cell types undergoing MT dys-function, is a promising avenue for therapeutic intervention in degenerative disease [1]. Mitochondrial donation has been demonstrated in multiple cell types, including neurons and myocytes. It has been shown to improve MT function and prevent apoptosis *in vitro*, as well as improve tissue repair *in vivo* [2-4].

Our lab studies MSC MT donation in the context of ortho-pedic disease, using *in vitro* chondrocyte cultures and explanted cartilage tissue as models. Using confocal imaging, we have identified several possible modes of MSC-chondrocyte MT transfer, including direct cell-cell contact (e.g., nanotubule-medial filipodial transfer, gap junction-mediated transfer) and what appears to be non-contact transfer, whereby MSCs release mitochondria into the extracellular space, which are then taken up by chondrocytes. We hypothesize that these are MT are packaged inside of extracellular vesicles (EVs) as so-called 'mitovesicles'.

This strategy of loading MT into EVs has precedent in literature. Phinney, et al., showed that MSCs can use mitovesicles, to outsource mitophagy of depolarized MT to macrophages, boosting bioenergetics for both the donating MSC and the recipient macrophage [5]. Furthermore, Morrison, et al., used cellular staining and flow cytometry to demonstrate that distressed lung epithelial cells can take up MT through EV-mediated transfer, and this ameliorates lung injury *in vivo* [6].

Our goal was to characterize the EVs produced by human MSCs. EVs are an inherently heterogenous population, making specific categorization difficult. However, it is widely recognized that they fall into three size categories: small (15-100 nm, exosomes), medium (150-1000, microvesicles), and large (1 μm+, apoptotic bodies).

We isolated EVs from human bone marrow derived MSCs and used dynamic light scattering (DLS) to analyze their size distribution (Figure 1). As expected, we found the three categories supported by previous work [7] (Figure 1).

Next, we used the Malvern NS300 NanoSight to identify which, if any of these categories, contain MT. We stained hMSC EVs with Mitotracker Red, then performed nanoparticle tracking analysis using the Nanosight's 565 nm fluorescent filter. We were able to validate that this method allows us to track exclusively EVs that contain mitochondrial content (Figure 2.)

Further, we found that mitovesicles make up around 20% of the total EV's released and appear to trend slightly larger than the general population (Figure 2.).

The significance of these findings is not yet clear, but likely reflects distinct modes of biogenesis and cargos for different sub-populations of mitovesicles.

Conclusions and Future Steps:

Our work thus far has confirmed our ability to isolate EVs from MSCs and identify mitovesicles within that population. Our next step is to identify and separate the EVs that contain functional and non-functional MT. This will allow us to begin identifying the role that these particles play in intercellular signaling and to further investigate MSC-EV mediated MT transfer.

References:

[1] Delco, M. L., Bonnevie, E. D., Bonassar, L. J., and Fortier, L. A. Mitochondrial dysfunction is an acute response of articular chondrocytes to mechanical injury. J. Orthop. Res. 36, (2018).

[2] Jiang, D., et al. Mitochondrial transfer of mesenchymal stem cells effectively protects corneal epithelial cells from mitochondrial damage. Cell Death Dis. 7, (2016).

[3] Konari, N., Nagaishi, K., Kikuchi, S., and Fujimiya, M. Mitochondria transfer from mesenchymal stem cells structurally and functionally repairs renal proximal tubular epithelial cells in diabetic nephropathy in vivo. Sci. Rep. 9, (2019).

[4] Spees, J. L., Olson, S. D., Whitney, M. J., and Prockop, D. J. Mitochondrial transfer between cells can rescue aerobic respiration. Proc. Natl. Acad. Sci. U. S. A. 103, (2006).

[5] Phinney, D. G., et al. Mesenchymal stem cells use extracellular vesicles to outsource mitophagy and shuttle microRNAs. Nat. Commun. 6, (2015).

[6] Morrison, T. J., et al. Mesenchymal stromal cells modulate macrophages in clinically relevant lung injury models by extracellular vesicle mitochondrial transfer. Am. J. Respir. Crit. Care Med. 196, (2017).

[7] Zhang, X., Hubal, M. J., and Kraus, V. B. Immune cell extracellular vesicles and their mitochondrial content decline with ageing. Immun. Ageing 17, (2020).
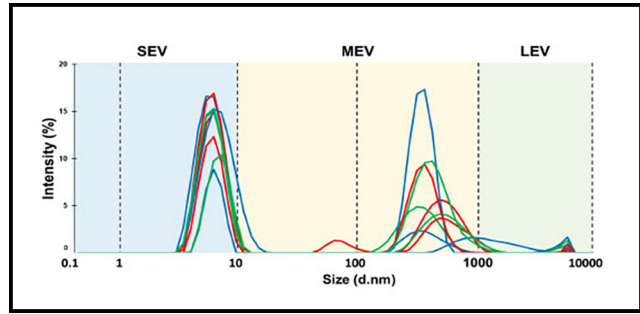
Figure 1: Dynamic Light Scattering of human MSC-derived extracellular vesicles (EVs) reveals three sub-populations of EVs based on size: small, (SEV; ~ 5-10 nm) medium, (MEV; ~ 100-1000 nm) and large (LEV; 5,000-10,000 nm). N = 3.
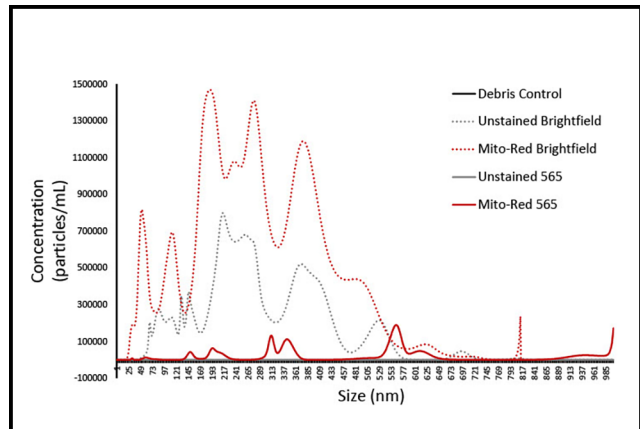

Figure 2: NTA supports trend of larger EVs containing MT. EVs were stained with Mitotracker Red and run with either a non-fluorescent (brightfield) filter, or with fluorescence exciting at 565 nm. These groups were compared to non-stained EVs and a double filtered PBS control. Unstained particles were undetectable using the 565 filter. Mitotracker positive EVs seemed to show a trend towards larger size, with nearly all of the smallest population disappearing altogether. N = 1.

Microfluidic Device to Study Breast Cancer Cell Migration

CNF Project Number: 2912-20
Principal Investigator(s): Claudia Fischbach
User(s): Siyoung Choi

Affiliation(s): Biomedical Engineering, Cornell University
Primary Source(s) of Research Funding: NIH
Contact(s): cf99@cornell.edu, sc2237@cornell.edu
Primary CNF Tools Used: Objet30 Pro 3D Printer

Abstract:

Bone metastasis through the dissemination of cancer cells worsens the prognosis of patients with advanced breast cancer. Migration of breast cancer cells is a fundamental process for breast cancer metastasis and is dependent on surrounding microenvironment. Cancer cell response to chemical signals and extracellular matrix (ECM) has been studied to understand the migration of cancer cells using microfluidic devices [1-2]. How bone ECM, mainly mineralized collagen, regulates breast cancer cell migration, however, is unclear.

Here, we utilized biomimetic approach in conjunction with microfluidic device to investigate the role of bone ECM on breast cancer migration.

Summary of Research:

Three-dimensional computer-aided design (3D CAD) software (Inventor, Autodesk) was used to design a microfluidic device for studying breast cancer migration. The device is composed of central channel for bone ECM deposition and two channels for chemical gradient and breast cancer cell seeding.

To guide the cancer cell entrance into the central channel, arrays of trapezoidal posts were placed between central channel and side channels (Figure 1). CNF's 3D printer (Object30 Pro, Stratasys) was used to fabricate a mold for this microfluidic device, casted with polydimethysiloxane (PDMS, Sylgard 184, Dow Corning) (Figure 2). To verify liquid flow within microfluidic channels, first, holes for liquid flow were punched at the end of each channel. Then, the PDMS microfluidic device and glass coverslip were treated with plasma cleaner and the channels of the device were bonded, facing the surface of a plasma treated glass coverslip for binding.

Aqueous solution containing red dye was injected at the inlet of each channel and filled all microfluidic channels (Figure 3). However, post structure of the device is not enough to provide high resolution and there are striation patterns in the microfluidic channel, which will be an issue for solution leakage (Figure 4).

Conclusions and Future Steps:

The 3D printer is a tool for fast and cost-effective fabrication. However, the resolution is limited to sub-millimeter structures of microfluidic devices.

To increase the resolution of our microfluidic device, a soft photolithography technique is required. In the future, an epoxy-based negative photoresist will be coated on a silicon wafer and patterned using a photomask.

References:

[1] Lab on a Chip (2017), Vol. 17, 3851.
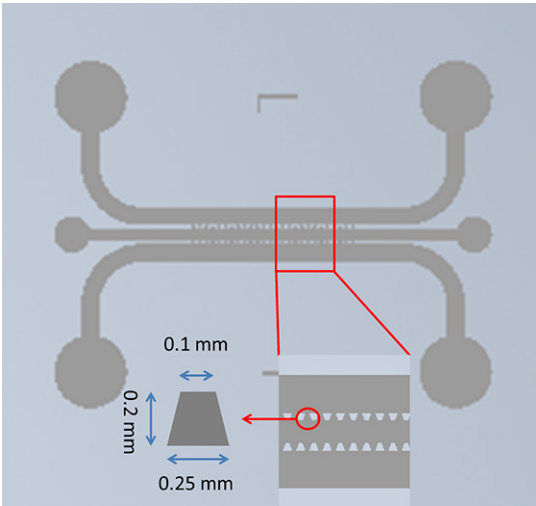[2] PNAS, 2012, Vol. 109, 13515.

Figure 1: Design and dimension of microfluidic device. The device is composed of three channels and the array of arrays of trapezoidal posts between channels will provide the entrance of breast cancer cells into bone ECM. The smallest dimension of posts is 100 μm.
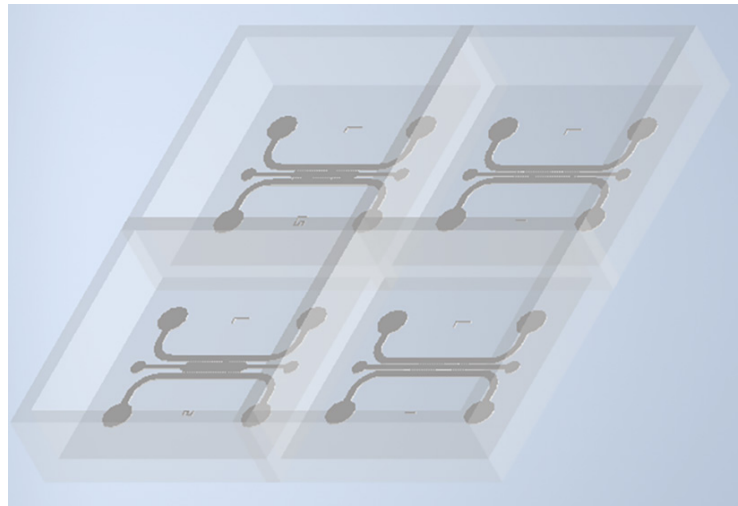

Figure 2: Mold design to cast PDMS microfluidic device. The mold has four microfluidic devices and each device has different central channel widths (1-2 mm).
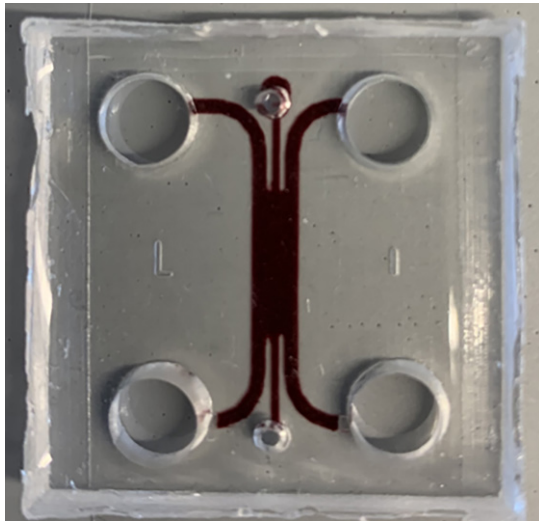

Figure 3: PDMS casted microfluidic device with fluidic channels. Plasma treated PDMS device was bound on plasma treated glass coverslip. Solution containing red dye was injected into holes of each channel.
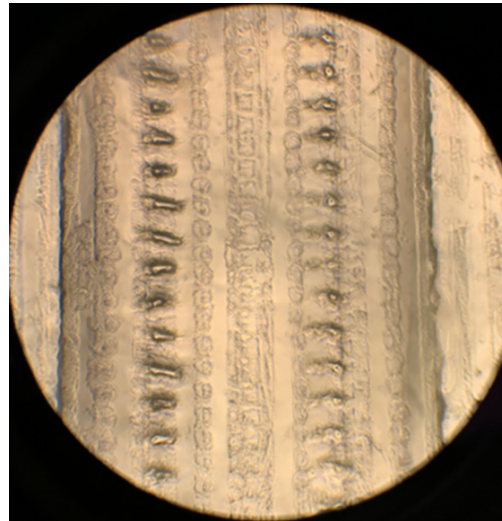

Figure 4: Low resolution of posts within central channel. Each post has different resolution and striation pattern was observed on the surface of PDMS device.